



Durham E-Theses

Electron spin resonance studies of doped rutile

Eggleston, Harold Simon

How to cite:

Eggleston, Harold Simon (1979) *Electron spin resonance studies of doped rutile*, Durham theses, Durham University. Available at Durham E-Theses Online: <http://etheses.dur.ac.uk/8943/>

Use policy

The full-text may be used and/or reproduced, and given to third parties in any format or medium, without prior permission or charge, for personal research or study, educational, or not-for-profit purposes provided that:

- a full bibliographic reference is made to the original source
- a [link](#) is made to the metadata record in Durham E-Theses
- the full-text is not changed in any way

The full-text must not be sold in any format or medium without the formal permission of the copyright holders.

Please consult the [full Durham E-Theses policy](#) for further details.

ELECTRON SPIN RESONANCE STUDIES OF DOPED RUTILE

By

HAROLD SIMON EGGLESTON, B.Sc. (DUNELM)

A thesis submitted to the Faculty of Science
of the University of Durham for the
Degree of Master of Science

Department of Applied Physics
and Electronics

Science Laboratories,

Durham.

November, 1979.

The copyright of this thesis rests with the author.
No quotation from it should be published without
his prior written consent and information derived
from it should be acknowledged.



ACKNOWLEDGEMENTS

I would like to express my sincere thanks to Dr. J S Thorp for his constant help and encouragement during this research project.

I am indebted to Professor G G Roberts for allowing me the use of the facilities of the department and to the technical staff, headed by Mr. F Spence, for their kind help.

I wish to thank Tioxide International Ltd., Stockton-on-Tees, for their award of a Research Studentship and their helpful cooperation during the course of this work.

My thanks also go to all my friends who, in various ways, have contributed to the success of this project ; and, finally, to Mrs. S Mellanby for typing this thesis.

CONTENTS

	<u>Page Nos</u>
ABSTRACT	1
CHAPTER ONE	
<u>INTRODUCTION</u>	1
CHAPTER TWO	
<u>CRYSTALLINE RUTILE</u>	3
2.1 UNIT CELL STRUCTURE	4
2.2 IMPURITY SITES	5
REFERENCES	8
CHAPTER THREE	
<u>EXPERIMENTAL TECHNIQUES</u>	9
3.1 ELECTRON SPIN RESONANCE	9
3.1.1 The Varian V4502-15 Spectrometer	9
3.1.2 E.S.R. 9 Cryostat	10
3.2 SAMPLE PREPARATION	11
3.3 THE SAMPLES	11
REFERENCES	13
CHAPTER FOUR	
<u>SINGLE CRYSTAL E.S.R. OF Fe/TiO₂</u>	14
4.1 SPIN HAMILTONIAN FORMALISM	14
4.2 THE Fe ³⁺ ION, (⁶ S _{5/2} , 3d ⁵)	17
4.3 RESULTS	20
REFERENCES	21
CHAPTER FIVE	
<u>COMPUTER SIMULATION OF POWDER LINESHAPES</u>	22
5.1 GENERAL THEORY OF POWDER SPECTRA	22
5.2 SOLUTION OF THE SPIN HAMILTONIAN	24
5.3 LINE BROADENING	31
5.4 EVALUATION OF THE EIGENVALUES	33
REFERENCES	35

	<u>Page Nos</u>
CHAPTER SIX	37
<u>APPROXIMATE CALCULATIONS OF Fe³⁺/TiO₂ POWDER SPECTRA</u>	
6.1 INTRODUCTION	37
6.2 NUMERICAL APPROACH	40
6.3 ANALYTICAL APPROACH	41
6.4 COMPUTATION	44
REFERENCES	47
CHAPTER SEVEN	49
<u>EXPERIMENTAL AND THEORETICAL POWDER LINESHAPES</u>	
<u>OF Fe/TiO₂</u>	
7.1 EXPERIMENTAL POWDER SPECTRA	49
7.1.1 Room Temperature	49
7.1.2 Liquid Helium Temperatures	49
7.2 COMPUTED SPECTRA	50
7.2.1 Results of Kneubuhl's Method (Ref.7.1)	50
7.2.2 Results of the Numerical Approach	51
7.3 CONCLUSIONS	51
7.3.1 Kneubuhl's Method	51
7.3.2 The Numerical Method	52
7.3.3 General Conclusions	52
REFERENCES	54
APPENDIX ONE	55
RESULTS OF MASS SPECTROSCOPY OF SAMPLES	

ABSTRACT

The Electron Spin Resonance Spectra at 9 GHz of iron doped rutile in both powder and single crystal form has been obtained at a variety of temperatures. The single crystal results have confirmed previous data ; the Fe^{3+} ion enters the lattice substitutionally for the Ti^{4+} ion and the spectrum exhibits a pronounced anisotropy.

The powders exhibited a variety of features not all of which were due to iron. The iron lines were identified both from the single crystals data and experimentally by comparing samples containing varying amounts of iron at several temperatures.

An approach to calculate the powder spectra from the Spin Hamiltonian was examined and discarded in favour of a faster, approximate, method. The latter assumed that the observed lines could be explained in terms of two separate transitions each with an effective spin of $S = \frac{1}{2}$. Using an analytical formula for the overall powder line shape gave rather poor results but a program based on calculating the lineshape numerically using the g^{-1} factor of Oasa and Vanngard gave good results.

This program can be used to simulate the spectra of other ions provided their behaviour can be approximated by transitions of spin $\frac{1}{2}$.

CHAPTER ONE

INTRODUCTION

Rutile is widely used as a pigment in paints. Studies have related some of its technological properties to trapping centres thought to be due to iron, nickel and a few other impurities. Some previous work on determining trap depths has been performed in the Department using Thermally Stimulated Conduction and Thermally Stimulated Luminescence as well as Electron Spin Resonance techniques.

In the latter method, the amplitude of new lines formed after optical irradiation was found to be related to the amplitudes of lines due to species such as Fe^{3+} and Ni^{2+} . By monitoring the decay rates of these lines following either thermal annealing or further (infra-red) optical activation, Hodgskiss (unpublished) showed that trap depths could be estimated. This method appears to have the advantage over optical methods that not only the trap depth can be found but also the nature of the trap.

All this previous work was with single crystal samples. In practice powders are used and so it is desirable to make similar studies of trapping centres directly in powdered pigments. As a first step in this direction it is essential to be able to correlate single crystal and powder E.S.R. spectra.

This work concerns only the Fe^{3+} ion. Firstly the single crystal Fe^{3+} spectrum was obtained and compared with published data. Next the various samples, both powdered single crystals and pigments, were examined and their spectra recorded. A method of simulating the powder spectra from the observed single crystal data was required and, after examining an approach utilizing the full spin Hamiltonian, a technique using the effective g values for each Kramers doublet was devised. This enabled



CHAPTER ONE

INTRODUCTION

Rutile is widely used as a pigment in paints. Studies have related some of its technological properties to trapping centres thought to be due to iron, nickel and a few other impurities. Some previous work on determining trap depths has been performed in the Department using Thermally Stimulated Conduction and Thermally Stimulated Luminescence as well as Electron Spin Resonance techniques.

In the latter method, the amplitude of new lines formed after optical irradiation was found to be related to the amplitudes of lines due to species such as Fe^{3+} and Ni^{2+} . By monitoring the decay rates of these lines following either thermal annealing or further (infra-red) optical activation, Hodgskiss (unpublished) showed that trap depths could be estimated. This method appears to have the advantage over optical methods that not only the trap depth can be found but also the nature of the trap.

All this previous work was with single crystal samples. In practice powders are used and so it is desirable to make similar studies of trapping centres directly in powdered pigments. As a first step in this direction it is essential to be able to correlate single crystal and powder E.S.R. spectra.

This work concerns only the Fe^{3+} ion. Firstly the single crystal Fe^{3+} spectrum was obtained and compared with published data. Next the various samples, both powdered single crystals and pigments, were examined and their spectra recorded. A method of simulating the powder spectra from the observed single crystal data was required and, after examining an approach utilizing the full spin Hamiltonian, a technique using the effective g values for each Kramers doublet was devised. This enabled

the observed spectra to be identified. The following chapters describe the steps in more detail.

CHAPTER TWO

CRYSTALLINE RUTILE

Titanium dioxide exists in three crystalline forms, brookite, anatase and rutile, details of which are given in Table 2.1 :

Type	Crystallographic System	Unit Cell Dimensions (nm)	Band Gap (eV)
Rutile	Tetragonal D_{4h}^{14}	a = 0.4594 c = 0.2958	3.03
Anatase	Tetragonal D_{4h}^{19}	a = 0.3783 c = 0.951	3.23
Brookite	Orthombic V_H^{15}	a = 0.5435 b = 0.9166 c = 0.5135	3.26

TABLE 2.1 : Structural forms of TiO_2

Amorphous TiO_2 can be precipitated from sulphate or chloride solutions, but hydrolysis by direct boiling of chloride solutions will produce rutile directly. Large crystals are grown by the Verneuil flame fusion method ; these crystals are black due to a large number of oxygen vacancies but after heating in oxygen become transparent with a slight yellow colour. These nonstoichiometric crystals of $Ti_{1+x}O_{2-x}$ may be semiconducting with a band gap depending on x while the 'pure' transparent, rutile crystals are insulators with a band gap of 3.03 eV. (2.8,2.9).

The work described in this thesis is concerned with titanium dioxide occurring in the rutile structural form.

2.1 UNIT CELL STRUCTURE

The tetragonal (001) axis is called the 'c' axis and the (010) and (100) axes are called the 'a' axes. The unit cell is shown in Fig.2.1 (Ref.2.1).

Each titanium atom is at the centre of a slightly distorted oxygen octahedron with principle axis in the (110), (001) and (110) directions. These provide a more useful axis system for discussing E.S.R. results and are labelled x,y,z respectively. They are shown in Fig. 2.2, where it can be seen that there are two different titanium sites differing only by a rotation of 90° about the c-axis (Ref.2.2), Table 2.2 shows the relation between the two axis systems and the two different sites.

Site	Direction	Axis
1	(001)	y (or 'c')
1	(110)	x
1	($1\bar{1}0$)	z
2	(001)	y (or 'c')
2	($1\bar{1}0$)	x
2	($\bar{1}\bar{1}0$)	z
Both	(100))	'a' axes
Both	(010))	

TABLE 2.2 : Axes in rutile single crystals

A convention is adopted in order to determine the direction of a magnetic field in the crystal two angles, θ and ϕ , are necessary.

Here θ is the angle between the field and the z axis and ϕ is the angle in the x-y plane between the x axis and the projection of the field in the x-y plane.

Rutile can be thought of as being formed by stacks of these octahedra parallel to the y (c) axis. Adjacent stacks are separated by open spaces, or channels, parallel to the 'y' axis which can be regarded as stacks of oxygen octahedra with the central titanium ion missing. Alternatively, rutile can be considered as being composed of layers of -O-Ti-O-O-Ti-O- chains, each layer perpendicular to the y axis and orientated at right angles to the layers immediately above and below.

2.2 IMPURITY SITES

Impurity ions may take up either substitutional or interstitial sites. Paramagnetic ions substituting for Ti^{4+} will have magnetic axes parallel to the x, y and z axes. As the lattice has two different titanium sites differing only by a rotation of 90° around the y axis, we would expect to see two E.S.R. spectra rotated by 90° about this axis (Fig. 2.2).

The existence of open channels parallel to the y axis results in easy diffusion of impurities in this direction. Ions may take up a position in the centre of these channels (Fig. 2.3). There are four of these interstitial sites (in Fig. 2.3) which differ only by a rotation of $\pm \alpha$ and $90 \pm \alpha$ where $\alpha = 12.6^\circ$, around the y axis (Ref 2.3). Thus for a paramagnetic ion distributed over these sites we would expect to see a four-fold E.S.R. spectrum with the principle axes along the y axes and in the x y plane, the latter axes making angles of $\pm \alpha$ and $90 \pm \alpha$ with the (110) directions. Small interstitial ions would not appreciably distort the lattice, Low and Offenbacher (Ref 2.4), first considered the space available to accommodate an ion at an interstitial site ; subsequently, having reviewed a recent set of ionic radii given

- Ti^{4+} ions
- O^{2-} ions

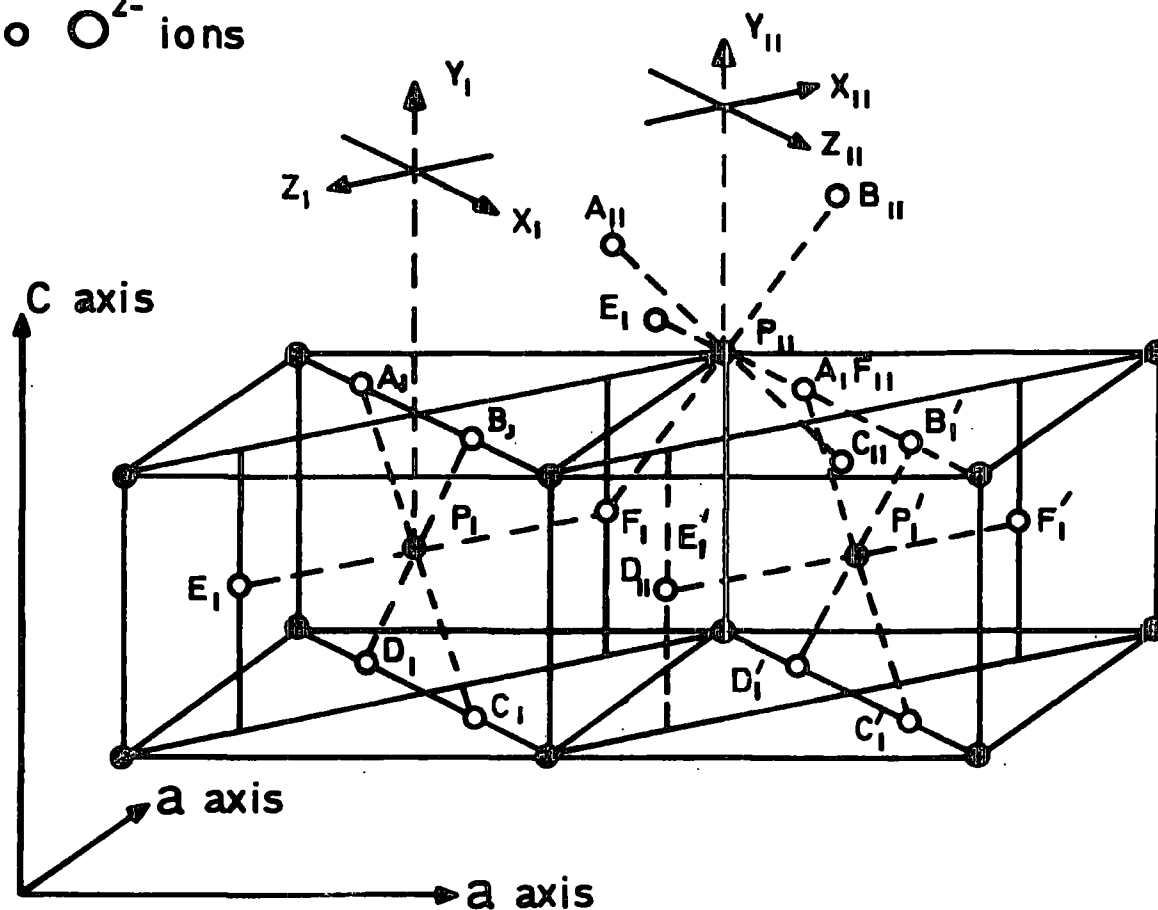
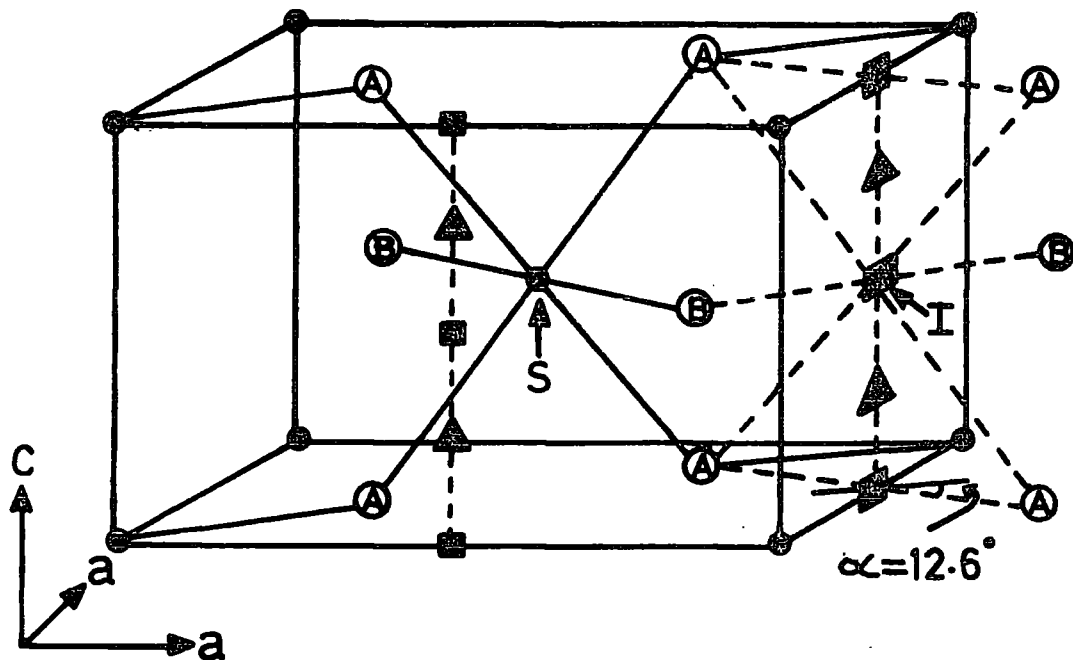


FIG. 2.2 CRYSTAL STRUCTURE AND AXIS OF SUBSTITUTIONAL SITES IN RUTILE. (AFTER ANDERSSON AND KOLBERG).



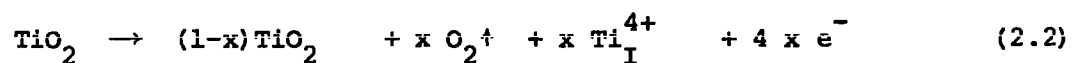
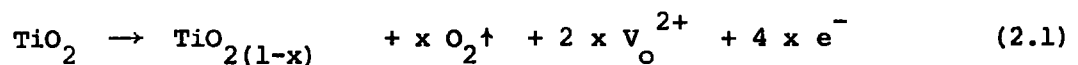
- Ti^{4+} $c = 2.959 \text{ \AA}$
- O^{2-} $a = 4.594 \text{ \AA}$
- $\frac{1}{2} \text{O} \frac{1}{2}$
- ▲ $\frac{1}{2} \text{O} \frac{1}{4}$

FIG. 2.3 CRYSTAL STRUCTURE OF RUTILE (TiO_2) SHOWING A UNIT CELL AND SOME $\frac{1}{2}\text{O}\frac{1}{2}$ (■) AND $\frac{1}{2}\text{O}\frac{1}{4}$ (▲) TYPE INTERSTITIAL SITES. THE POSITION AROUND THE OCTAHEDRALLY CO-ORDINATED SUBSTITUTIONAL ION S AND AROUND THE INTERSTITIAL SITE I ARE INDICATED. (AFTER KERSSEN AND VOLGER).

by Shannon and Prewitt (Ref 2.5), Kersen & Volger (Ref 2.3) concluded that ions with radii in the region of 0.63 - 0.82 Å might prefer these interstitial positions.

Huntington and Sullivan (Refs 2.3, 2.6) suggested the existence of a second-class of interstitial sites on $\frac{1}{2}, 0, \frac{n}{4}$ type positions with n odd (i.e. points marked A in Fig 2.3). These sites are surrounded by four O^{2-} ions, two at a distance of 1.77 Å and two at 1.74 Å. Energy calculations for the two types of sites showed that the difference in energy between the occupancy of one type of site or the other is small and might depend on the charge and radius of the interstitial ion. A four-fold E.S.R. spectrum could be expected also from ions in this type of site with an angle $\alpha \approx 12.6$. For all impurity positions the spectra can be uniquely characterized by the g values along the principle axes and the angle α , i.e. g_x, g_y, g_z and α . For substitutional ions $\alpha = 0$.

Rutile shows large variations from stoichiometry. When heated in a reducing atmosphere (vacuum, hydrogen, CO or titanium powder) rutile loses oxygen and becomes a n-type semiconductor. (The as-grown crystals need to be heated in O_2 as mentioned above). Two reducing reactions have been thought possible:-



where V_O is an oxygen vacancy,

Ti_I is an interstitial titanium ion.

(the V_O or Ti_I can capture one or more electrons).

Initially, it was thought that the first reaction dominated but later E.S.R. results showed the presence of interstitial Ti^{3+} ions.

To explain the results of many different experiments, both processes have to be used. Which predominates depends on the temperature, atmosphere and partial pressure of oxygen when the sample is reduced. However, it appears that $V_O - Ti_I^{3+}$ and $Ti_I^{3+} - Ti_I^{3+}$ complexes form and more exotic formations have been suggested to explain all the results (Ref 2.3).

The main impurity ions found in rutile are listed in Table 2.3 (Ref 2,3). Iron enters the lattice as substitutional Fe^{3+} , while nickel can be either Ni^{3+} or Ni^{2+} . Gerritsen and Sabrisky (Ref.2.10) estimate that about 90% of the nickel is interstitial Ni^{2+} and the rest is Ni^{3+} which can enter the lattice in either interstitial or substitutional positions.

Ionic Species	Ionic Radius (Å)	Isotope	Natural Abundance (%)	Nuclear Spin	Nuclear Moments (μ_n)
O^{2-}	1.36	^{16}O	99.5	0	
		^{18}O	0.5	0	
Mg^{2+}	0.72	^{24}Mg	78.7	0	
		^{25}Mg	10.1	$\frac{5}{2}$	- 0.885
		^{26}Mg	11.2	0	
Al^{3+}	0.530	^{27}Al	100.0	$\frac{5}{2}$	+ 3.64
Si^{4+}	0.400	^{28}Si	92.2	0	
		^{29}Si	4.7	$\frac{1}{2}$	- 0.55
		^{30}Si	3.1	0	
		^{46}Ti	8.0	0	
Ti^{3+}	0.67	^{47}Ti	7.3	$\frac{5}{0}$	- 0.79
Ti^{4+}		0.605	^{48}Ti	74.0	0
Fe^{3+}	0.645	^{49}Ti	5.5	$\frac{7}{2}$	- 1.10
		^{50}Ti	5.2	0	
		^{54}Fe	5.8	0	
		^{56}Fe	91.6	0	
		^{57}Fe	2.2	$\frac{1}{2}$	< 0.05
Cu^{2+}	0.72	^{58}Fe	0.3	0	
		^{63}Cu	69.1	$\frac{3}{2}$	2.23
		^{65}Cu	30.9	$\frac{3}{2}$	2.38

TABLE 2.3 Properties of ions which are usually present in rutile (after Kersen and Volger).

REFERENCES

CHAPTER TWO

- 2.1 A Von Hippel, J. Kalnajo and W.B. Westphal, 'Protons, Dipoles and Charge Carriers in Rutile', J. Phys. Chem. Solids, 23 (1962) 779.
- 2.2 P-Olof Andersson, Erik Kollberg, 'E.P.R. Spectra of Iron Doped Rutile', Phys. Rev. B 8 (1973) 4956.
- 2.3 J. Kerksen and J. Volger, 'E.P.R. Study of Slightly Reduced Rutile Crystals', Physica 69 (1973) 535.
- 2.4 L. Low and E.L. Offenbacher, 'E.S.R. of Magnetic Ions in Complex Oxides', Review of results in Rutile... Solid State Phys. 17 (1965) 135.
- 2.5 Shannon and Prewitt, Acta. Cryst. B 25 (1969) 925.
- 2.6 M. Huntington and G. Sullivan, Phys. Rev. Lett. 14 (1965) 177.
- 2.7 D. Carter & A. Okaya, 'E.P.R. of Fe³⁺ in TiO₂ (Rutile)' Phys. Rev. 118 (1960) 1485.
- 2.8 F. A. Grant, 'Properties of Rutile (TiO₂)', Rev. Mod. Phys. 31 (1959) 646.
- 2.9 Cronmeyer, 'Properties of Rutile Single Crystals' Phys. Rev. 87 (1965) 876-86.

CHAPTER THREE

EXPERIMENTAL TECHNIQUES

3.1 ELECTRON SPIN RESONANCE

All the measurements were performed on a Varian V4502-15 X-band spectrometer. Figure 3.1 shows a block diagram of the instrument. Low temperature measurements were possible using an Oxford Instrument E.S.R.9 Liquid Helium cryostat system which produced temperatures in the range 3.8 K \rightarrow 300 K.

3.1.1 The Varian V4502-15 Spectrometer (Ref. 3.1)

Figure 3.1 outlines the instrument. An X-band cavity is placed in between the pole pieces of the electromagnet. The sample is suspended in the centre of the cavity inside a "spectrosil" quartz tube. The special tube is used to ensure that there are no extra lines due to ions in the quartz. The spectrometer has a 12" electromagnet controlled by a VFR 5203 field regulated power supply which incorporates the 'field-dial' system. This is claimed by the manufacturer to be capable of setting the desired field to 0.1 mT with 1 part in 10^5 repeatability and a resolution of 0.002 mT. This was checked using a proton magnetometer and it was found that although the repeatability was good there was a small error in the field scale. The scale was good enough for identifying lines but when accurate field measurements were required the proton magnetometer was used.

A Klystron is used to generate the microwaves. The output is taken, along a waveguide, to a hybrid tee. The hybrid tee will not allow microwave power to pass in a straight line from arm 1 to arm 4. Instead, the power is divided equally between arms 2 and 3. If all the power is absorbed and non reflected then the crystal detector in arm 4 receives

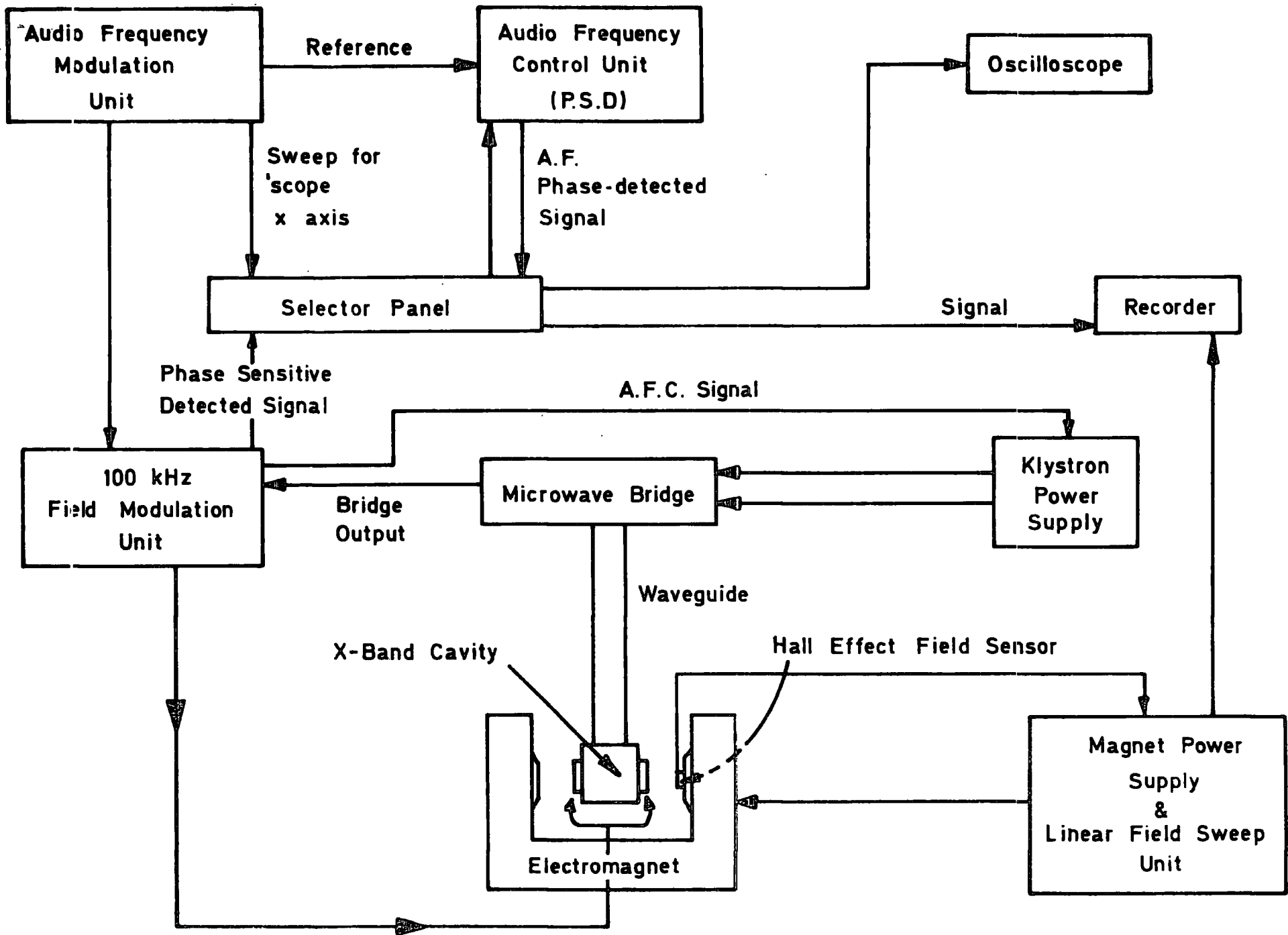


FIG 2.1 BLOCK DIAGRAM OF ESR SPECTROMETER

no power. Thus it forms a bridge which becomes unbalanced when the power absorbed in one arm alters. Arm 3 is connected to a resistive load and arm 2 through an attenuator to the sample cavity. In practice the crystal detector used produces less noise if it operates with a constant bias, so the bridge is unbalanced, by adjusting the load in arm 3.

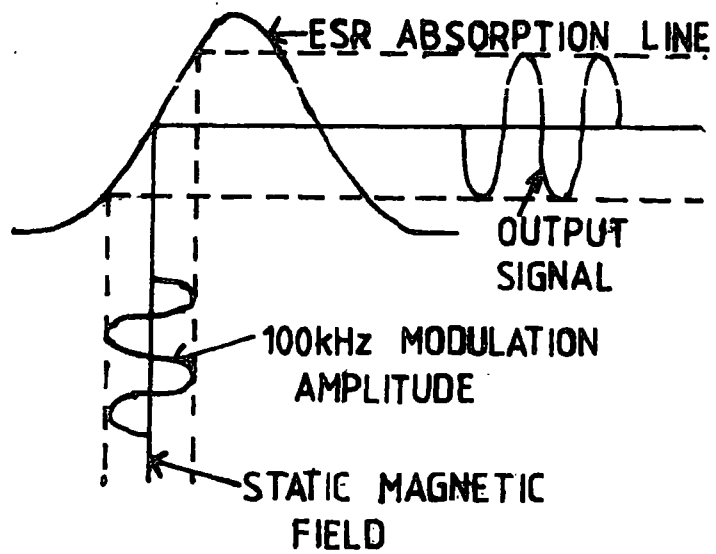
An A.F.C. system is incorporated using a 10 kHz oscillator, which modulates the Klystron power supply and the resultant 10 kHz modulation of the frequency is detected through a phase sensitive detector. The phase of the detected signal depends on whether the Klystron centre frequency is above or below the absorption frequency of the cavity and so an error signal can be produced to correct the Klystron frequency.

The walls of the cavity contain a pair of coils which are used to modulate the magnetic field. These coils are fed from a 100 kHz oscillator, which also provides a reference for a phase sensitive detector. The output from the bridge travels through a preamplifier and a narrow band 100 kHz amplifier to the phase sensitive detector (Fig. 3.2 a). This technique enables much better signal-to-noise ratios to be obtained. The signal-to-noise ratio may also be improved by increasing the time taken for the field to sweep through the range being examined. This is only possible when the feature under examination does not change with time. If the amplitude of the modulation is too big, then the line is distorted and broadened (Fig. 3.2b and c), (Ref. 3.2, 3.3, and 3.4).

The output recorded on a chart recorder is the differential of the absorption line.

3.1.2 E.S.R.9 Cryostat

The E.S.R.9 is a continuous flow cryostat designed to be operated from 3.8 K up to 300 K. The liquid helium is sucked out of its flask through a syphon into a stainless steel feed capillary which takes the coolant through the body of the cryostat to the bottom of the quartz tube.



a) SIGNAL RESULTING FROM FIELD MODULATION

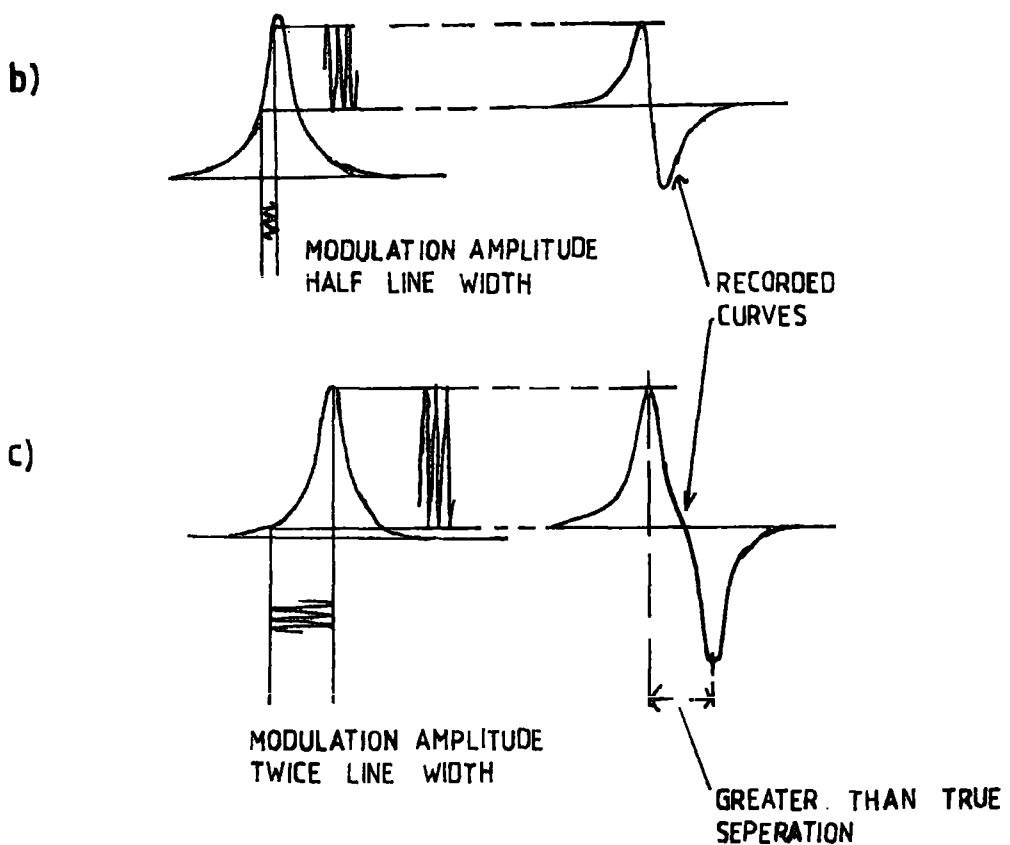


FIG 32 OPERATION OF FIELD MODULATION OF AN E.S.R. SPECTROMETER.

It flows past a heater thermocouple and over the sample. The coolant then flows out of the sample tube and returns to the syphon entry arm via the annular space around the feed capillary and the helium return line. The helium is sucked through the cryostat by a diaphragm pump to avoid contamination by pump oil. The temperature can be controlled by adjusting both the gas flow rate and the heater current. The temperature can be controlled by an Oxford Instruments D.T.C.2 temperature controller so that the temperature remains constant, within the accuracy it can be measured, while the E.S.R. lines are recorded.

3.2 SAMPLE PREPARATION

The boules were aligned using a Laue back-reflection camera and then cut (using a diamond wheel) into cubes about 1 x 2 x 2 mm. The alignment was checked using Laue photographs and between crossed polarizers in a microscope. This also checked the perfection of the crystals. If the Laue photographs showed blurred spots then the crystal lattice was distorted. In the case of the Nakasumi Boule double spots were observed indicating a grain boundary in the path of the X-ray beam with a mis-orientation of $\approx 1.5^\circ$ degrees. Observing the crystals under the microscope also revealed one cube with a crack separating two slightly misorientated regions. This resulted in a doubling of the line in the E.S.R. spectra.

Samples of each boule were analysed using mass spectroscopy by Tioxide International at their Central Laboratories, Stockton-on-Tees. Table 3.1 lists the main impurities and Appendix 1 gives a complete list of the analysis results.

3.3 THE SAMPLES

A number of samples were examined and are listed below :

(a) National Lead Boule.

This boule had been bought from the National Lead Company for previous experiments in this department and some suitable sized pieces were examined. Unfortunately, there was not enough left to powder so only single crystal analysis was possible. The iron concentration was 0.01%.

(b) "Swiss" Boule.

This boule had been heavily doped with iron for use in a maser experiment. The concentration varied from 0.05% at the centre of the boule, where it was yellow, to 1.5% at the edge, where the crystal was a deep red colour. The red parts were the first to be powdered to obtain a powder spectrum due to their high Fe^{3+} concentration.

(c) Pigments.

These pigments were given by Tioxide International and contained about 25 ppm Fe. They had differing Al_2O_3 concentrations and had been subjected to varying degrees of heat treatment. They did not appear to have an iron spectra although they contained 0.0025% iron.

(d) Nakasumi Boule.

This boule had a low Al_2O_3 concentration but it was strained and contained grain boundaries and so no detailed examination of its spectra was performed due to the differing orientations in even small off-cuts.

TABLE 3.1 :

Main Impurities in Samples Examined.

	National Lead	Swiss Boule (3)		Tioxide Pigments ¹		
		<u>centre</u>	<u>side</u>	A	C	E
%Al ₂ O ₃	1.0	0.007	0.03	0.61 ²	3.28 ²	1.56 ²
%SiO ₂	0.1	0.05	0.06	0.6	0.6	0.6
%Fe	0.01	0.05	1.5	.0025	.0035	.0025
NiO ppm	100	≤ 9	≤ 20	≤ 3	-	-
Cr ₂ O ₃	≤ 6	≤ 10	≤ 8	1	2	2
Ca O	20	20	200	10	15	8
MgO	400	70	90	6	20	12
Zr O ₂	30	100	200	15	20	<2
Zn O	≤60	500	200	1	10	3
P ₂ O ₅	-	800	500	8	25	8
Bi	-	10	500	-	-	-
%SO ₃	0.4	0.2	0.2	-	-	-

Notes:- (1) Sample B, D and F were the same as A,C and E respectively except that they had been heated at 600° C for 30 minutes.

(2) These figures were obtained from chemical analysis and knowledge of the starting constituents. The figures from mass spectrometry were A = 1%, C = 2%, E = 1.5% reflecting the inaccuracy of mass spectrometry at these high levels of dopant.

(3) See text.

REFERENCES

CHAPTER THREE

- 3.1 Varian V4502 E.P.R. Spectrometer Manual.

- 3.2 Spectroscopy at Microwave and Radio Frequencies.
D. Ingram, pub. Butterworths.

- 3.3 Electron Spin Resonance, Poole, Interscience 1977.

- 3.4 H.M. Assenheim, Introduction to E.S.R.
Adam-Hilger 1966.

CHAPTER FOUR

SINGLE CRYSTAL E.S.R. OF Fe/TiO₂

4.1 SPIN HAMILTONIAN FORMALISM

A free ion with a total angular momentum, J , placed in a magnetic field will have energy levels given by :-

$$W = g\beta H M_J \quad (4.1)$$

where W = Energy

β = Bohr magneton

H = Magnetic field

M_J = Angular momentum quantum number

g is the Landé factor given by (Ref 4.1) :-

$$g = 1 + \frac{J(J+1) + S(S+1) - L(L+1)}{2J(J+1)} \quad (4.2)$$

L = Orbital angular momentum

S = Spin angular momentum

If an alternating field of frequency ν is placed at right angles to H , photons will be absorbed if :-

$$h\nu = g\beta H \quad (4.3)$$

and $M_J = \pm 1$ as these are the only allowed transitions. Experimentally it is found to be more convenient if ν is kept constant and H is varied to find the absorption. If there is only one electron (i.e. $L = 0$) then

$g = 2.00229$. The difference from 2 is due to small corrections which can be calculated using quantum electrodynamics.

When a paramagnetic ion is placed in a solid it will interact with neighbouring ions in one, or both, of two ways :

- (a) Interactions between the magnetic dipoles
- (b) Interactions between the paramagnetic ion and neighbouring diamagnetic ions.

In doped rutile the distances between the paramagnetic ions will, in general, be considerably larger than the distance between paramagnetic ions and diamagnetic ions. Thus the predominant interaction is the second. The charge of the diamagnetic ion sets up strong internal fields which, to a good approximation, can be considered to be static. This internal field is called the crystal or ligand field.

The crystal field has a large effect on the ions. Firstly, it lifts the degeneracy of the ground state forming a number of new levels. This is called the zero-field splitting. The splitting, and number of components, depends on the symmetry and strength of the crystal field. In the 3d, or iron group, the crystal field is of moderate strength being larger than the spin-orbit coupling but smaller than the Coulomb interaction. The crystal field changes the resonance condition and absorption can take place at several values of field. This is called the fine structure. Other interactions which can effect the energy levels include the hyperfine structure which is due to interactions between the electrons and the nucleus with a non-zero nuclear spin.

A 'g' value can be defined by eqn. 4.3. In general this 'g' value will be different from the Landé splitting factor and to minimize confusion is called the spectroscopic splitting factor. As the crystal field has a certain symmetry, the 'g' value will not be isotropic and in the most general case 'g' can be represented by g_{ij} , which can be

called, rather loosely, a tensor.

The behaviour of the energy levels is conventionally represented by a Spin Hamiltonian; this includes terms which are spin dependent but neglects those which only add a constant to the energy of the levels, since we are only interested in the differences between the levels.

A Spin Hamiltonian can be derived by considering the different interactions and summing various contributions. These interactions are; Coulombic forces between both electrons and electrons and the nucleus, also between electrons with the crystal field, spin-orbit and spin-spin interactions, the Zeeman term which is responsible for paramagnetism, electron nuclear forces, a nuclear contribution and a term due to diamagnetism (Ref 4.2) The Coulombic forces are independent of field and can be neglected, the Zeeman term is the dominant one which concerns us. The crystal field gives rise to the fine structure and is also very important in rutile. The other terms represent small corrections and can be ignored. The nuclear spin of iron is 0 (Table 2.3), and so there are no hyperfine contributions. A reasonably general Spin Hamiltonian, which represents the observed energy levels, is (Refs 4.2,4.3).

$$H = \beta \underline{S} \cdot \underline{g} \cdot \underline{H} + \underline{S} \cdot \underline{D} \cdot \underline{S} \quad (4.4)$$

where \underline{S} = Electron spin operator
 \underline{H} = Applied magnetic field
 \underline{g} = Spectroscopic splitting
 \underline{D} = Fine Structure interaction tensor

In this approximation terms, due to higher order fine structure interactions, have been ignored.

4.2 THE Fe³⁺ ION, (⁶S_{5/2}, 3d⁵)

The impurity sites in rutile have orthorhombic symmetry and the Spin Hamiltonian must have the same symmetry. A general spin Hamiltonian for S state ions in orthorhombic symmetry without any hyperfine interactions is (4.5,4.4)

$$\begin{aligned} \mathcal{H} = & \beta g_{ij} \underline{H} \cdot \underline{S} + D \left[S_z^2 - \frac{S}{3} (S+1) \right] + E(S_x + S_y) + \\ & + \frac{a}{6} \left[S_x^4 + S_y^4 + S_z^4 - \frac{S}{5} (S+1) (3S^2 + 3S-1) \right] \\ & + \frac{F}{180} \left[35 S_z^4 - 30 S (S+1) S_z^2 + 25 S_z^2 - 6S(S+1) + 3S^2 (S+1)^2 \right] \end{aligned} \quad (4.5)$$

where D and E are fine structure constants and a and F are due to quadrupole interactions.

Other higher order terms exist, but are of little importance. In fact, the E.S.R. spectra of many impurity S state ions in rutile are adequately described by including just the first three terms.

In equation (4.5) the first term can be simplified. The \underline{g} factor is represented by a 3 x 3 matrix, g_{ij} , (which is not a true tensor quantity). The quantity g_{ij} can then be diagonalized by a suitable similarity transform which is equivalent to changing the principle axes of the matrix. In Section 2 the use of a set of axes x, y, z, was described. Using these as the principle axis, g_{ij} is diagonal, i.e.

$$g_{ij} = 0 \quad i \neq j \quad (4.6)$$

$$g_{11} = g_x, \quad g_{22} = g_y, \quad g_{33} = g_z$$

so that g_{ij} can be represented by a vector \underline{g}_i . In fact in Fe/TiO₂

$g_x = g_y = g_z$ so that g_i can become a numerical constant (Ref. 4.6).

Exact diagonalization of (4.5) would be very difficult to perform. To determine the angular variation of the levels computer methods are used.

Iron, in a trivalent state, substitutes for Ti^{4+} as shown in Fig 2.3. As there are two sites differing only by a rotation of 90° about the y axis, the E.S.R. spectra exhibits, in general, two lines for each transition.

Fe^{3+} has spin $5/2$ and so an isolated ion will have a six-fold degenerate ground state. In rutile, the degeneracy is lifted by the crystal field and three pairs of levels are formed. These levels are Kramers doublets and the remaining degeneracy is lifted by an applied magnetic field (Figs. 4.1, 4.2). The levels can be labelled $\pm \frac{1}{2}$, $\pm \frac{3}{2}$, $\pm \frac{5}{2}$ in order of ascending energy but these do not strictly represent the spins of the level because the states are admixtures of spin states of the form

$$a \left| \left(s = \frac{1}{2} \right) \right\rangle + b \left| \left(s = -\frac{3}{2} \right) \right\rangle + c \left| \left(s = \frac{5}{2} \right) \right\rangle \text{ or } d \left| \left(s = -\frac{1}{2} \right) \right\rangle + e \left| \left(s = \frac{3}{2} \right) \right\rangle + f \left| \left(s = -\frac{5}{2} \right) \right\rangle = |A\rangle$$

where A is a label for one of the observed levels. Another way of labelling the states is 1, 2...6 in order of ascending energy and this leads to less confusion.

This explains why transitions between $+\frac{3}{2} \rightarrow -\frac{3}{2}$ are observed. The states are not pure spin states so the forbidden $\Delta m = 2$ transition can occur through mixtures of appropriate spins.

The Spin Hamiltonian used to describe the observed spectra is (4.3)

$$\begin{aligned} \mathcal{H} = & g \underline{H} \cdot \underline{S} + D \left[S_z^2 - \frac{35}{12} \right] + E \left(S_x^2 - S_y^2 \right) + \frac{a}{6} \left(S_x^4 + S_y^4 + S_z^4 - \frac{707}{16} \right) \\ & + \frac{7}{36} F \left[S_z^4 - \frac{95}{14} S_z^2 + \frac{81}{16} \right] \end{aligned} \quad (4.7)$$

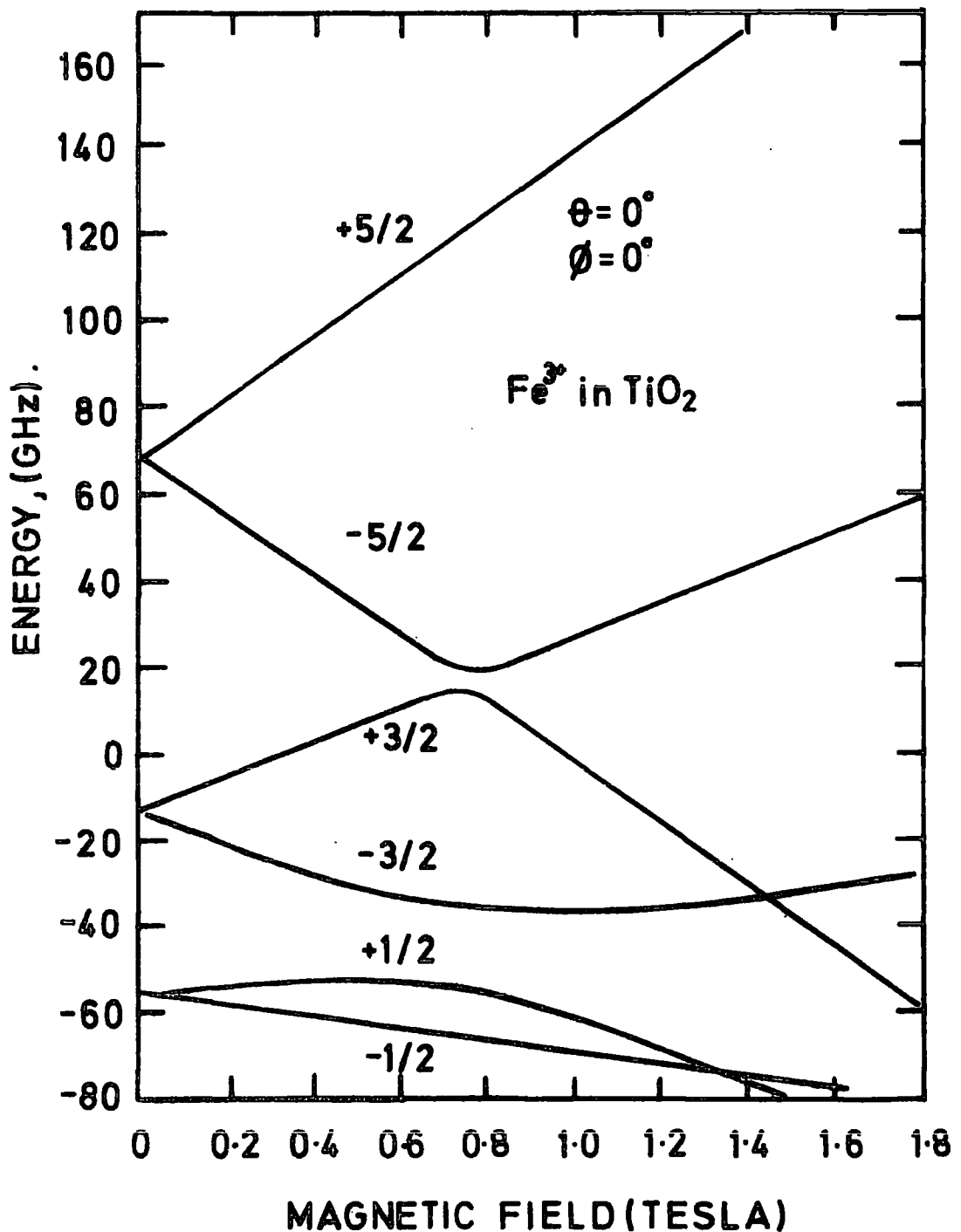


FIG. 4.1. CALCULATED ENERGY LEVELS AS A FUNCTION OF FIELD STRENGTH FOR THE FIELD IN THE Z DIRECTION ($\theta=0^\circ$, $\phi=0^\circ$). THE NUMBERS ON THE LEVELS ARE FOR IDENTIFICATION. (AFTER D.L.CARTER AND A.OKAYA).

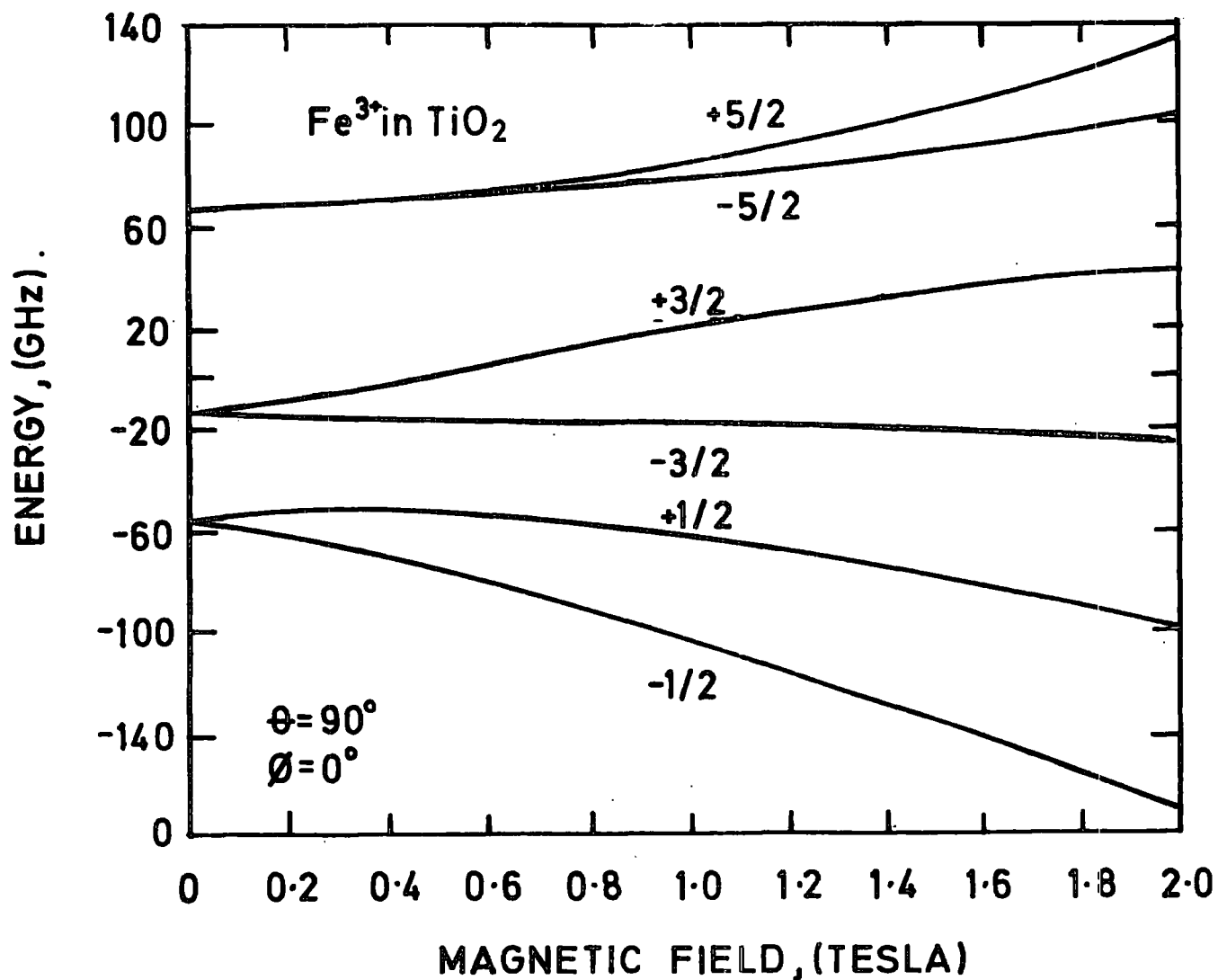


FIG. 4.2. CALCULATED ENERGY LEVELS AS A FUNCTION OF FIELD STRENGTH FOR THE FIELD IN THE X DIRECTION ($\theta=90^\circ$, $\phi=0^\circ$). THE NUMBERS ON THE LEVELS ARE FOR IDENTIFICATION (AFTER D.C. CARTER AND A. OKAYA)

The constants have been derived experimentally by various authors and a comparison is made in Table 4.1. Lichenberger and Addison^(4.7) included in their Spin Hamiltonian a term

$$C \left[\left(7 S_z^2 - \frac{35}{4} \right) (S_x^2 - S_y^2) + (S_x^2 - S_y^2) \left(7 S_z^2 - \frac{35}{4} \right) \right]$$

but as they conclude that the constant C equals 0.000 there is no need to consider it further.

Carter and Okaya's values give better results at, or near, zero field and they claim that the signs of their constants agree with intensity measurements between 1.4 and 4.2 K. These are the values which shall be used.

Experimentally, frequencies of about 9 GHz were used. The photon energy is too small to stimulate transitions between different doublets (except at fields far higher than could be used) so only three transitions could be seen. Fig 4.3 shows an isofrequency plot of Carter and Okoya at 7.07 GHz. Only two transitions can be seen. This is because the transition probability between the $+\frac{5}{2}$ and $-\frac{5}{2}$ states is small and the population of these states is less than for lower levels, so we would not expect to see it at all.

In analyzing the experimental results, it appears that the $\pm \frac{3}{2}$ transition could not be seen with the magnetic field along the y ('c') axis. In Fig. 4.4 the explanation becomes clear. The separation between these two levels increases until it reaches a maximum of about 8 GHz and then decreases again with increasing magnetic field. Thus the microwave radiation is unable to stimulate transitions in the range being considered.

Additional spectra resulting from complexes of Fe^{3+} and an interstitial proton and Fe^{3+} and a nearby oxygen vacancy have also been reported^(4.9).

Parameter	Carter & Okoya ^(4.6) (1960)	Schollmeier ^(4.8) (1966)	Lichenberger & Addison ^(4.7) (1969)	Units
g	2.000 ± 0.005	2.000 ± 0.005	2.000 ± 0.005	
D	20.35 ± 0.01	20.35 ± 0.01	20.38 ± 0.01	GHz
E	2.21 ± 0.07	2.21 ± 0.07	2.06 ± 0.01	GHz
F	-0.5 ± 0.3	-0.5 ± 0.3	0.68 ± 0.02	GHz
a	1.10 ± 0.1	+1.10 ± 0.1 (diag elements)	-0.84 ± 0.04	GHz
		-1.10 ± 0.1 (off diag elements)		GHz
C	-	-	0.00 ± 0.01	GHz

TABLE 4.1 Spin Hamiltonian Parameters for Fe³⁺/TiO₂.

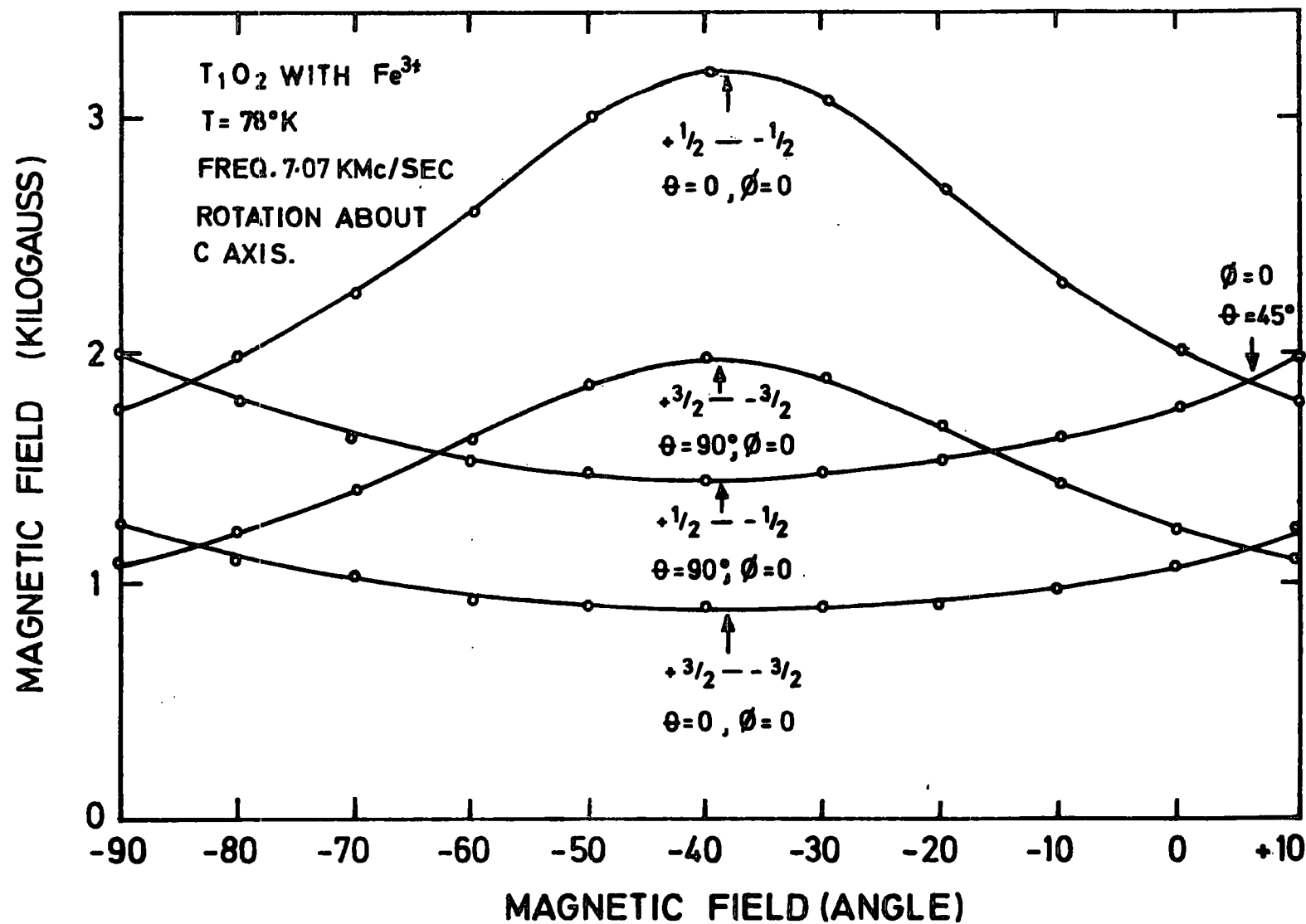


FIG.4.3 EXPERIMENTAL VALUES OF MAGNETIC FIELD FOR RESONANCE AS A
 FUNCTION OF ANGLE IN THE (001) PLANE FOR A FIXED FREQUENCY
 OF 7.07 KMc/SEC.

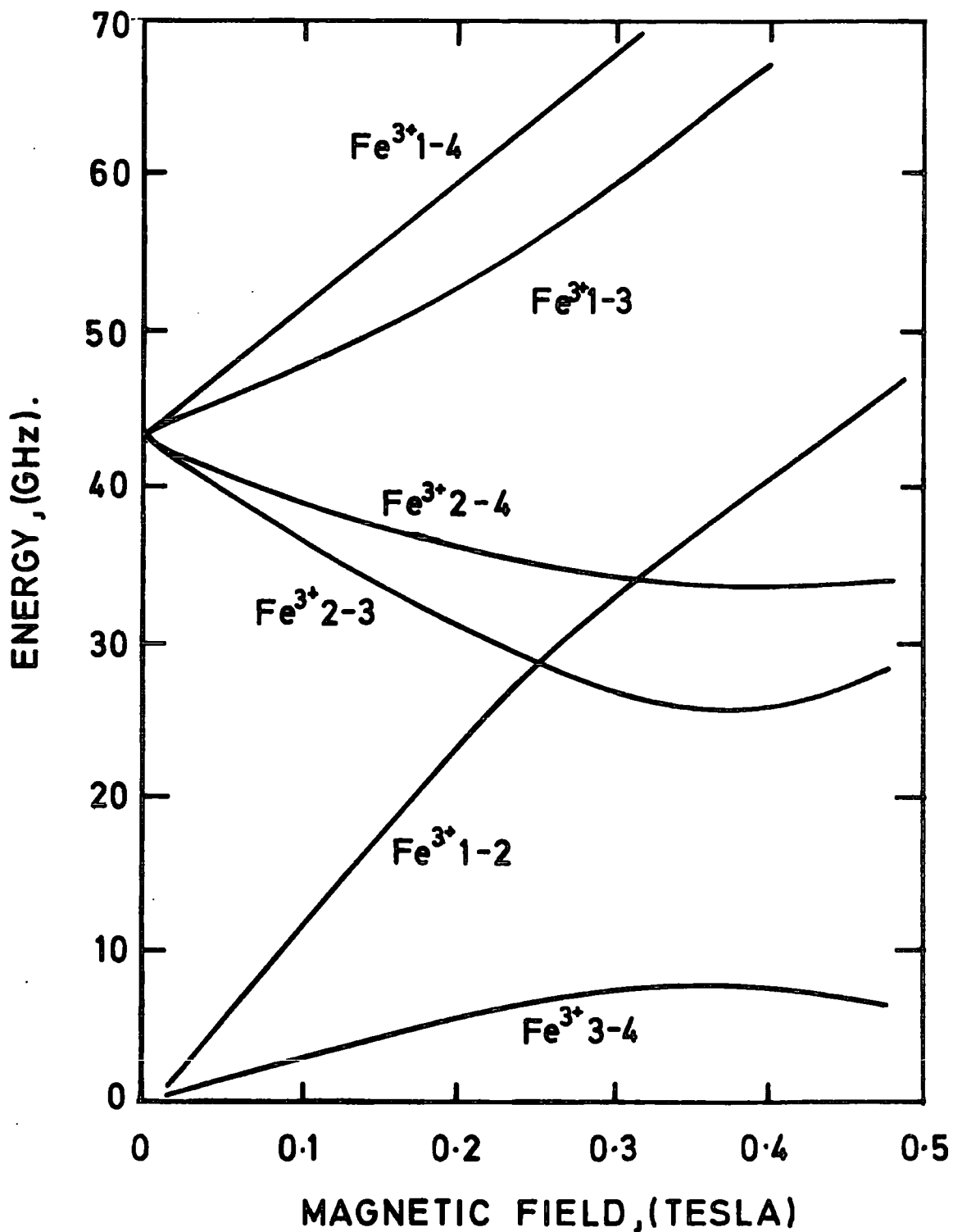


FIG. 44. ISOGON PLOT OF THE Fe^{3+} SPECTRUM FOR THE MAGNETIC FIELD ALONG THE c AXIS.

Several single crystal specimens were examined and the resulting spectra investigated. Figures 4.5 and 4.6 are from the same crystal with the magnetic field at right angles. This sample, the Swiss Boule, had a large iron concentration of the order of a few per cent. In Figure 4.5 the four lines can be clearly seen, the two larger lines are from the $\pm \frac{1}{2}$ transition and the two smaller ones from the $\pm \frac{3}{2}$ transition. Figure 4.6 has one large line due to the $\pm \frac{1}{2}$ transition as the signals from the two sites coincide with the magnetic field parallel to the c' axis. The reason no $\pm \frac{3}{2}$ transition is seen is explained in Section 4.2. In Figure 4.6 several smaller signals can be seen. These could not be investigated completely (due to their small amplitude) but comparison between their behaviour in the x-y plane and the isofrequency plots published by Andersson and Kollberg, suggest that the three lines occurring with the field greater than 0.2 Tesla are due to a substitutional iron ion perturbed by a nearby interstitial proton and the fourth line of comparable size is due to a Fe^{3+} ion with a nearby Ti^{4+} interstitial ion.

Figure 4.7 shows the observed spectrum of a crystal with about 0.01% iron. (This figure was obtained from a mass spectroscopy performed on a sample of the same boule by B.T.P. at their laboratories in Stockton). The gain was about 100 times greater and several other elements gave large lines. The spectra due to Cr^{3+} and Ni^{3+} were identified. There appeared to be a very wide feature at about 0.3 Tesla. This was present in all the samples, even the swiss boule where it could be seen at high gain. Its magnitude appears to be independent of dopants and it is entirely isotropic. It was also seen in powder samples. Andersson and Kolberg report a similar feature and suggest that it is related to trapped electrons. An experimental isofrequency plot is shown in Figure 6.1.



FIG. 4.5 Spectrum of single crystal Fe/TiO_2 ; (001) plane, 9.096 GHz. (High Fe concentration)

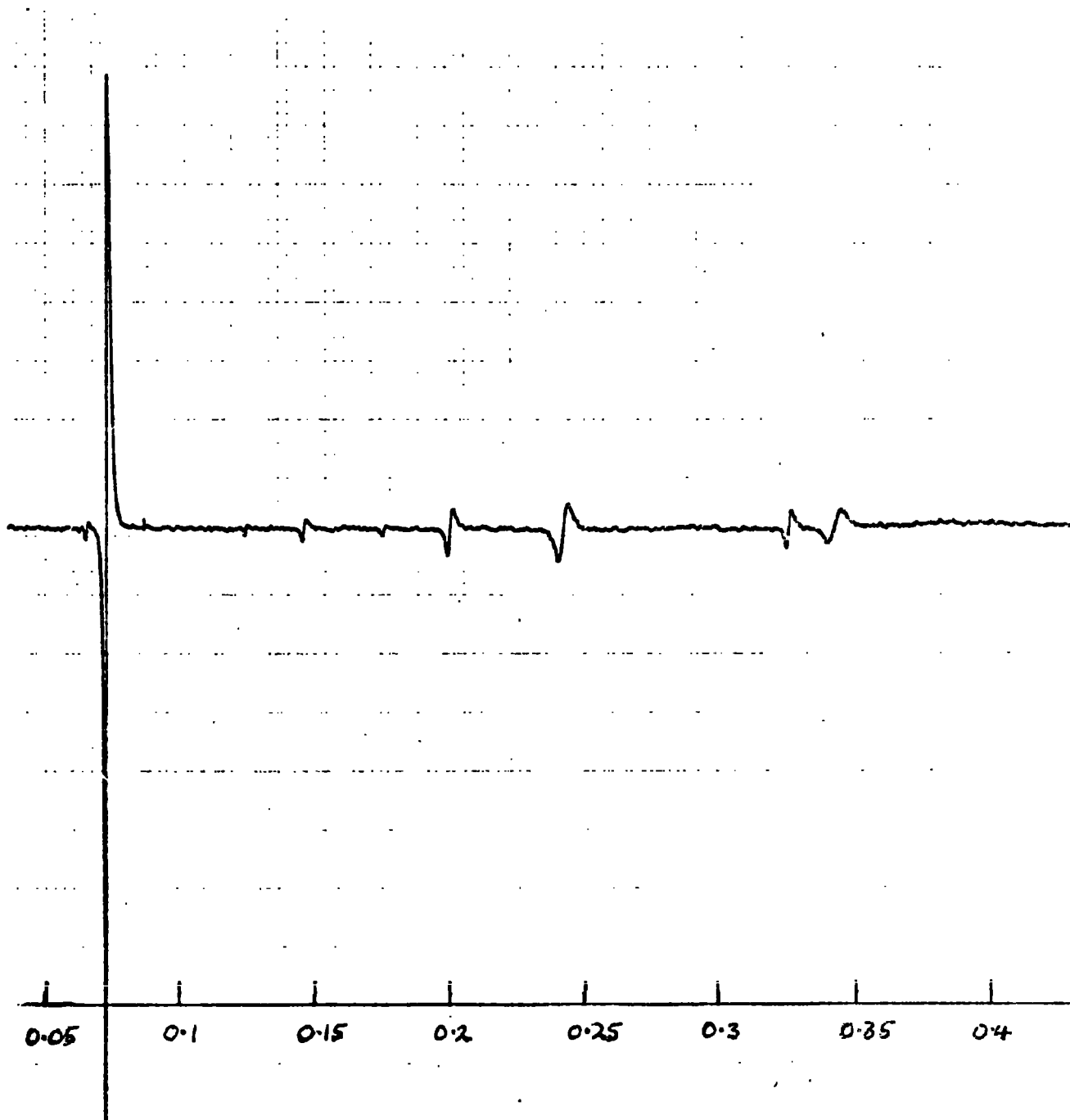


FIG. 4.6 Spectrum of single crystal Fe/TiO_2 ;
H//c, 9.096 GHz. (High Fe concentration).

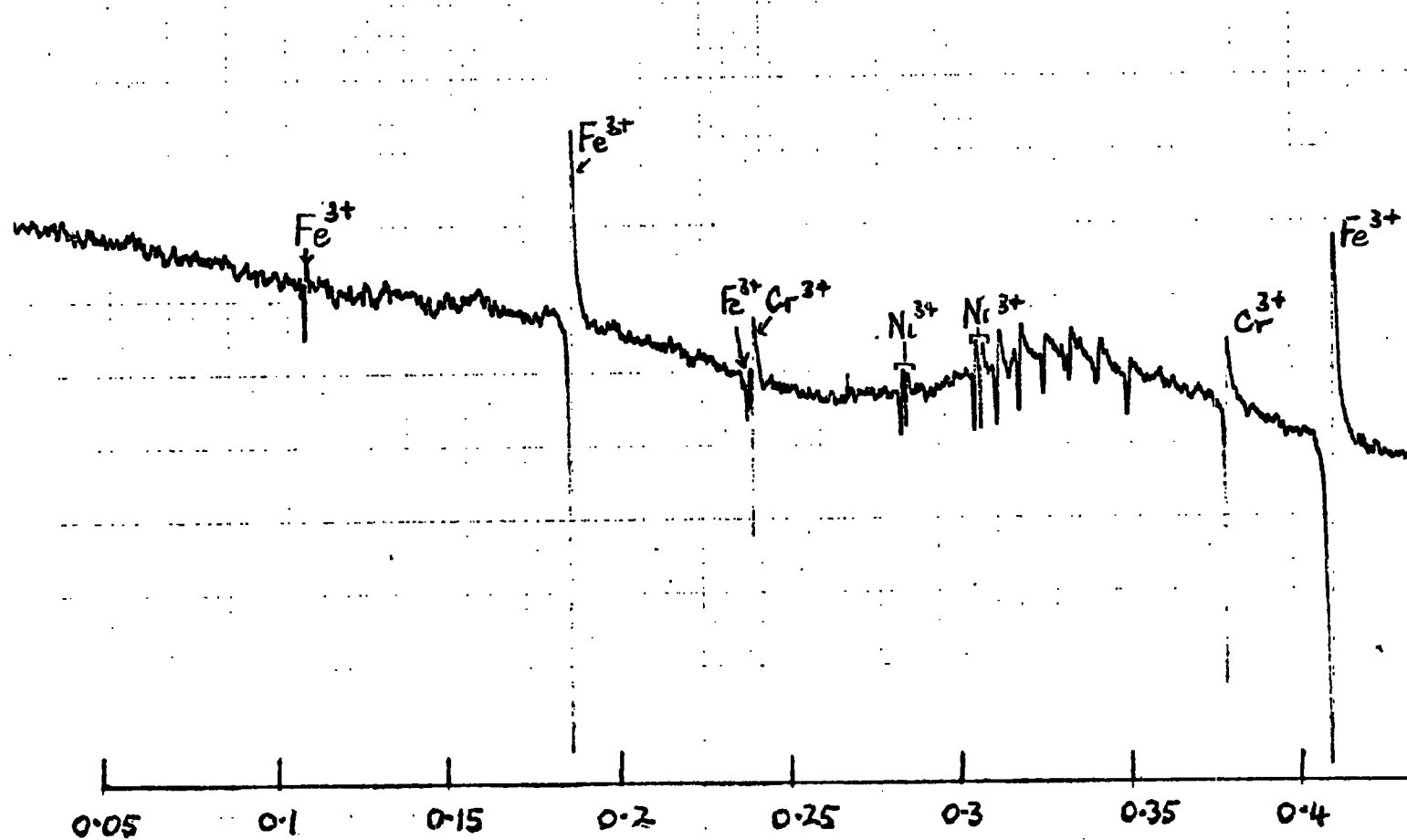


FIG. 4.7 Spectrum of single crystal Fe/TiO_2 , (low Fe concentration) showing other species ;
 H in (001) plane, 9.0975 GHz.

REFERENCES

CHAPTER FOUR

- 4.1 A. Abragam and B. Bleaney, "E.P.R. of Transition Ions"
Clarendon Press (1970).
- 4.2 P. C. Taylor, J.F. Bougher, H.M. Kritz, "Magnetic Resonance
in Polycrystalline Solids", Chem. Rev. 75 (1975) 203.
- 4.3 H. M. Assenheim, "Introduction to E.S.R.", Adam Hilger (1966).
- 4.4 Bleaney and Trenham,
Proc. Roy. Soc (London) A205 (1951) 135.
- 4.5 B. Bleaney and K. W. Stevens, "Paramagnetic Resonance",
Rep. Prog. Phys. 16 (1953) 108.
- 4.6 D. Carter and Okaya, "E.P.R. of Fe^{3+} in TiO_2 (Rutile)",
Phys. Rev. 118 (1960) 1405.
- 4.7 Lichenberger and Addison, "F-and X-band spectroscopy on
 Fe^{3+} in Rutile", Phys. Rev. 184 (1964) 381.
- 4.8 Scholleneier, Proc. IEEE, 54 (1966) 1485.
- 4.9 Per-Olof Andersson and E. Kolberg, "Extra E.P.R. Spectra of
Iron Doped Rutile", Phys. Rev. B8 (1979) 4956.
- 4.10 W.E.Hughes, C.C.Johnson, and L.E.Rouger, "Eigenvalues for the
Spin Hamiltonian for Fe^{3+} in TiO_2 ", NASA Report TMX 63359,
(August 1968).

CHAPTER FIVE

COMPUTER SIMULATION OF POWDER LINESHAPES

Powder lineshapes can be derived from the Spin Hamiltonian. This approach is outlined below, but because it is so time consuming other techniques, using various approximations, have been used to display the basic features of the observed powder spectra.

In the experimental ranges used, (fields from 0-0.5 T and frequencies of about 9 GHz), the approximations appear to be valid and lead to no serious discrepancies. The techniques outlined are more generally applicable but are discussed specifically in terms of Fe/TiO₂.

5.1 GENERAL THEORY OF POWDER SPECTRA

In outlining the principles of the theory the following assumptions will be made :-

- (a) The powder particles are randomly orientated
- (b) Hyperfine splitting is ignored
- (c) Line broadening, due to dipole-dipole and exchange interactions, are initially ignored, (their influence is discussed later).

The energy levels of the system are determined by the diagonalization of eqn. 4.7. Once the levels are known the separations, equal to the absorbed quantum of energy $h\nu$, can be easily calculated. This leads to a resonance condition of the form

$$h\nu = f(H) \tag{5.1}$$

The absorption at a particular field H is given by a shape

function $S(H)$ which is normalized such that

$$\int_0^{\infty} S(H) dH = 1 \quad (5.2)$$

The function $S(H)$ is given by the probability of crystalites being able to absorb in the region H to $H + dH$, i.e. (Ref. 5.1, 5.2 and 5.3).

$$S(H) dH = \sum_{\Omega}^{-1} \int_H^{H+dH} \ell_m(\Omega) d\Omega(H_m) \quad (5.3)$$

The equation is integrated over all elements of solid angle such that $H < H_m < H + dH$ where H_m is the appropriate resonance condition

$H_m = H_m(\mu, \phi)$ where $\mu = \cos\theta$ and

$$d\Omega = d\mu d\phi = \sin\theta d\theta d\phi \quad (5.4)$$

The summation is over the two different cases, the $\pm \frac{1}{2}$ and the $\pm \frac{3}{2}$ transitions.

The factor $\ell_m(\Omega)$ is the transition probability and if it is independent of Ω it can be taken out of the integral. In rutile the change in transition probability with change in θ and ϕ is not large so this can, to a reasonable approximation, be taken outside the integral, and because of the normalization equation (5.2) it is set equal to 1. Also equation 5.3 is a double integral with $F(H-H')$ the appropriate Gaussian, Lorentzian or Voigt broadening function (see Section 5.3). However, there are few instances when $F(H-H')$ is dependent on orientation and in rutile it can also be taken outside the integral.

Each transition can be evaluated separately and the two resulting shape functions summed to give the final shape function $S'(H)$. This is then convoluted with the appropriate line broadening equation to give the observed spectra.

We can now rewrite equation (5.3) as :

$$S(H) = \Omega^{-1} \int_H^{H+dH} (dH)^{-1} d\Omega \quad (5.5)$$

5.2 SOLUTION OF THE SPIN HAMILTONIAN

The single crystal spectra may be calculated by inserting in \mathcal{H}_{sp} , the Spin Hamiltonian the appropriate parameters and finding the eigenfunctions and eigenvalues by the normal quantum mechanical methods. The time dependent (transition-inducing) interaction with a monochromatic field (H_0) is included to first order, using semi-classical perturbation theory (Ref. 5.5).

Calculation of single crystal E.S.R. spectrum is equivalent to solving, for fixed values of the static applied field, H_0 and H_1 , the time dependent Schrödinger equation:-

$$\mathcal{H}_{sp} |\psi(t)\rangle = -i \hbar \frac{\partial}{\partial t} |\psi(t)\rangle \quad (5.6)$$

If \mathcal{H}_{sp} can be written as $\mathcal{H}_{sp} = \mathcal{H}_{stat} + \mathcal{H}_{rad}$, where \mathcal{H}_{stat} is a large time independent term and \mathcal{H}_{rad} a small time dependent term, one would first solve the static case.

$$\mathcal{H}_{stat} |v_k\rangle = E_k |v_k\rangle \quad (5.7)$$

and then include \mathcal{H}_{rad} ; Eqn 5.6 is solved in the approximation that $|\psi(t)\rangle$ is a linear combination of the stationary eigenstates $|v_k\rangle$ with time-dependent coefficients so that the population of the states are linear functions of the duration of application of \mathcal{H}_{rad} , (Ref.5.4).

Suppose that $|\mathbf{v}_k\rangle$ is expanded in a complete set of orthonormal states (basis vectors) $|u_m(j)\rangle$, which are eigenfunctions of J^2 and J_z (eigenval. $j(j+1)$ and m respectively) with J being the angular momentum operator as usual. Then

$$|\mathbf{v}_k\rangle = \sum_m |u_m(j)\rangle \langle u_m | \mathbf{v}_k \rangle \quad (5.8)$$

(This is equivalent to expanding an ordinary 3.D vector in a basis $\underline{e}_1, \underline{e}_2, \underline{e}_3$ as $\underline{v} = \underline{e}_1 (\underline{e}_1 \cdot \underline{v}) + \underline{e}_2 (\underline{e}_2 \cdot \underline{v}) + \underline{e}_3 (\underline{e}_3 \cdot \underline{v})$, except that the scalar products $\langle u_m | \mathbf{v}_k \rangle$ are in a complex Hilbert space). If the Hamiltonian can be written in terms of angular momentum operators :-

$$\mathcal{H} |\mathbf{v}_k\rangle = |\mathbf{v}_e\rangle = \sum_{mm'} |u_{m'}(j)\rangle \langle u_m | \mathcal{H} | u_m \rangle \langle u_m | \mathbf{v}_k \rangle \quad (5.9)$$

$$\text{where } \langle u_{m'} | \mathcal{H} | u_m \rangle = \mathcal{H}_{mm'} \equiv \int u_{m'}^*(j) \mathcal{H} u_m(j) d\tau \quad (5.10)$$

is a matrix element of \mathcal{H} . Now $|\mathbf{v}_e\rangle$ is a vector in the space spanned by $|u_m\rangle$ so :-

$$|\mathbf{v}_e\rangle = \sum_{m'} |u_{m'}(j)\rangle \langle u_{m'} | \mathbf{v}_e \rangle \quad (5.11)$$

and using (5.9) and (5.11) $|\mathbf{v}_e\rangle = \mathcal{H} |\mathbf{v}_k\rangle$ can be written :-

$$\langle u_{m'} | \mathbf{v}_e \rangle = \sum_m \langle u_{m'} | \mathcal{H} | u_m \rangle \langle u_m | \mathbf{v}_k \rangle \quad (5.12)$$

where the coefficients $\langle u_m | \mathbf{v}_k \rangle$, ($m = j, j-1, \dots, -j$), may be thought of as a column vector ; for example the basis vectors are the set

$$\begin{bmatrix} \delta_{j,m} \\ \delta_{j-1,m} \\ \vdots \\ \delta_{-j,m} \end{bmatrix}$$

Using this notation (5.7) can be rewritten as

$$\sum_m \langle u_{m'} | \mathcal{H}_{\text{stat}} | u_m \rangle \langle u_m | v_k \rangle = E_k \langle u_{m'} | v_k \rangle \quad (5.13)$$

Consider the set of eigenvectors $\langle u_m | v_k \rangle$ for all eigenvalues E_k . These are orthogonal, i.e.,

$$\sum_m \langle v_e | u_m \rangle \langle u_m | v_k \rangle = \delta_{ek} \quad (5.14)$$

hence the set $\langle u_m | v_k \rangle$

may be written as the columns of a unitary matrix, U_{mk} , and may be written

$$\sum_m \mathcal{H}_{m'm} U_{mk} = E_k U_{m'k} \quad (5.15)$$

Using equation (5.14),

$$\sum_{m', m} U_{lm'}^\dagger \mathcal{H}_{mm'} U_{mk} = \sum_{m'} U_{lm'} U_{m'k} E_k = \delta_{lk} E_k = D_{lk} \quad (5.16a)$$

or,

$$U^\dagger \mathcal{H}_{\text{stat}} U = D \quad (5.16b)$$

Thus to solve equation (5.7) the problem reduces to finding the unitary transformation which reduces the Hermitian matrix $\mathcal{H}_{\text{stat}}$ (element $\mathcal{H}_{mm'}$) to diagonal form with elements $E_k \delta_{lk}$.

Equation (5.6) can be written,

$$\sum_k a_k(t) \langle v_j | \mathcal{H}_{\text{rad}}(t) | v_k \rangle = -i\hbar \sum_k \dot{a}_k(t) \langle v_j | v_k \rangle = -i\hbar \dot{a}_j(t) \quad (5.17)$$

We want a solution of (5.17) with $\mathcal{H}_{\text{rad}}(t) = \mathcal{H}_{\text{rad}}(0) e^{i\omega t}$ and

$a_j(t=0) = 1, a_k(0) = 0, k \neq j$. The corresponding form of (5.17) is :-

$$\ddot{a}_j(t) = -(i\hbar)^{-1} \sum_k a_k(t) e^{i\omega t} \langle v_j | \mathcal{H}_{\text{rad}}(0) | v_k \rangle \quad (5.18)$$

which may be solved by standard methods (Ref. 5.4) to give :-

$$I_{jk} \propto |\langle v_j | \mathcal{H}_{\text{rad}}(0) | v_k \rangle|^2 \quad (5.19)$$

where I_{jk} is the intensity of the transition from state k to state j

or the power absorbed in the resonance line $k \rightarrow j$. To reduce (5.19)

to matrix notation we use (5.8) to give

$$\begin{aligned} \langle v_j | \mathcal{H}_{\text{rad}} | v_k \rangle &= \sum_{mm'} \langle v_j | u_{m'} \rangle \langle u_{m'} | \mathcal{H}_{\text{rad}}(0) | u_m \rangle \langle u_m | v_k \rangle \\ &= \sum_{m'm} U_{jm'}^+ \mathcal{H}_{\text{rad}}(0)_{m'm} U_{mk} \\ &= (U^+ \mathcal{H}_{\text{rad}}(0) U)_{jk} \end{aligned}$$

so

$$I_{jk} \propto |(U^+ \mathcal{H}_{\text{rad}}(0) U)_{jk}|^2 \quad (5.20)$$

In a typical E.S.R. experiment, the oscillating field, $H_1 e^{i\omega t}$ is perpendicular to the static field H . With $\mathcal{H}_{\text{rad}} = \mathcal{H}_1 e^{i\omega t}$ the transition probability connecting the states k and j has been taken as (Ref. 5.13).

$$I_{jk}^2 = |\langle v_j | \mathcal{H}_1 | v_k \rangle|^2 / (\beta H_1)^2 \quad (5.21)$$

To simulate E.S.R. spectra I_{jk} has to be multiplied by a shape function $S(H)$ normalized such that :-

$$\int S(H) dH = 1 \quad (5.22)$$

However, from time dependent perturbation theory the transition probability is a frequency dependent quantity (Ref. 5.14) given by $I_{jk}^2 f(\nu)$, with $\int f(\nu) d\nu = 1$. Since the E.S.R. spectrometer works at a constant frequency, the intensity integrated over the magnetic field becomes :-

$$\int I_{jk}^2 S(H) dH = \int I_{jk}^2 f(\nu) \frac{dB}{d\nu} d\nu \quad (5.23)$$

For narrow lines $I_{jk}^2 \frac{dB}{d\nu}$ can be taken as a constant over the line width and the integrated intensity becomes $I_{jk}^2 \frac{dB}{d\nu}$, which is the factor that should multiply a normalized shape function $S(B)$ in simulations of E.S.R. spectra.

In cases where $S > \frac{1}{2}$ the situation is complicated because $\frac{dB}{d\nu}$ depends on the field. In the next chapter we will use an effective spin of $S = \frac{1}{2}$ and a resonance condition $h\nu = g \beta H$, which implies that $\frac{dB}{d\nu}$ is proportional to $\frac{1}{g}$. We can now define an intensity factor, W ,

$$W = \frac{I_{jk}}{g} \quad (5.24)$$

This factor was pointed out by Aasa and Vanngard in 1975 (Ref. 5.13) and has been used by some authors to improve their simulated spectra (Ref. 5.15, 5.16). Even if I_{jk} is assumed to be a constant, the variation in W due to the $1/g$ dependence should be included in any calculations. The effect of using it is shown in Chapter 7, where the simulation is considerably improved.

Thus from (Ref. 5.16b) and (5.20) the energy levels, and the magnitude of the transition between them may be computed. Dowsing and Gibson (Ref. 5.6) and Oasa (Ref. 5.7) have used a Spin Hamiltonian of the form

$$\mathcal{H} = \underline{H} \cdot \underline{g} \cdot \underline{S} + D \left[S_z^2 - \frac{1}{3} S(S+1) \right] + E \left[S_x^2 - S_y^2 \right] \quad (5.25)$$

to describe a d^5 ion without any hyperfine interaction (i.e. Fe^{3+}).

They use computational procedures to solve this equation and have derived powder spectra from it. Fe^{3+} , in a substitutional site in rutile needs two further terms to adequately describe its behaviour and these terms combined with the facts that g is isotropic and $s = 5/2$ (Section 4.2) give :-

$$\begin{aligned} = g \underline{H} \cdot \underline{S} + D \left[S_z^2 - \frac{32}{12} \right] + E \left[S_x^2 - S_y^2 \right] + \frac{a}{6} \left[S_x^4 + S_y^4 - \frac{707}{10} \right] \\ + F \left[S_z^4 - \frac{95}{14} S_z^2 + \frac{81}{16} \right] \end{aligned} \quad (5.26)$$

To rewrite this in an Energy Matrix form we must replace the operators by their matrix representations discussions of matrix representations of spin and angular momentum operators given in most text books (e.g. Dicke & Wittke (Ref. 5.8)). They give the following relations :-

$$\left[S_- \right]_{m_s, m_s'} = \sqrt{(s - m_s') (s - m_s' + 1)} \delta_{m_s, m_s' - 1} \quad (5.27)$$

$$\left[S_+ \right]_{m_s', m_s} = \left[S_- \right]_{m_s, m_s'} \quad (5.28)$$

$$\left[S_z \right]_{m_s, m_s'} = m_s' \delta_{m_s, m_s'} \quad (5.29)$$

where \underline{S}_+ and \underline{S}_- have the usual definitions of "step-up" and "step-down" operators.

$$\underline{S}_x = \frac{1}{2} (\underline{S}_+ + \underline{S}_-) \quad (5.30)$$

$$\underline{S}_y = \frac{-i}{2} (\underline{S}_+ - \underline{S}_-) \quad (5.31)$$

Substituting for $s = 5/2$ we find :-

$$\underline{S}_x = \begin{pmatrix} 0 & \sqrt{5}/2 & 0 & 0 & 0 & 0 \\ \sqrt{5}/2 & 0 & \sqrt{2} & 0 & 0 & 0 \\ 0 & \sqrt{2} & 0 & 3/2 & 0 & 0 \\ 0 & 0 & 3/2 & 0 & \sqrt{2} & 0 \\ 0 & 0 & 0 & \sqrt{2} & 0 & \sqrt{5}/2 \\ 0 & 0 & 0 & 0 & \sqrt{5}/2 & 0 \end{pmatrix} ; \underline{S}_y = i \begin{pmatrix} 0 & -\sqrt{5}/2 & 0 & 0 & 0 & 0 \\ \sqrt{5}/2 & 0 & -\sqrt{2} & 0 & 0 & 0 \\ 0 & \sqrt{2} & 0 & -3/2 & 0 & 0 \\ 0 & 0 & 3/2 & 0 & -\sqrt{2} & 0 \\ 0 & 0 & 0 & \sqrt{2} & 0 & -\sqrt{5}/2 \\ 0 & 0 & 0 & 0 & \sqrt{5}/2 & 0 \end{pmatrix}$$

$$\underline{S}_z = \begin{pmatrix} 5/2 & 0 & 0 & 0 & 0 & 0 \\ 0 & 3/2 & 0 & 0 & 0 & 0 \\ 0 & 0 & 1/2 & 0 & 0 & 0 \\ 0 & 0 & 0 & -1/2 & 0 & 0 \\ 0 & 0 & 0 & 0 & -3/2 & 0 \\ 0 & 0 & 0 & 0 & 0 & -5/2 \end{pmatrix} \quad (5.32)$$

These are substituted into equation (5.26) and the resulting matrix is shown in Table 5.1. To find the energy levels for an arbitrary applied magnetic field the field has to be reduced into its components along the x, y and z axes and then substituted into the matrix of Table 5.1 This matrix was diagonalized using approximations to be described in chapter six.

	5/2	3/2	1/2	-1/2	-3/2	-5/2
5/2	$\frac{5}{2} G_z + \frac{10}{3} D$ $+ \frac{a}{2} + \frac{F}{3}$	$\frac{\sqrt{5}}{2} (G_x - iG_y)$	$\sqrt{10} E$	0	$\frac{\sqrt{5}}{2} a$	0
3/2	$\frac{\sqrt{5}}{2} (G_x + iG_y)$	$\frac{3}{2} G_z - \frac{2}{3} D$ $-\frac{3}{2} a - F$	$\sqrt{2} (G_x - iG_y)$	$3\sqrt{2} E$	0	$\frac{\sqrt{5}}{2} a$
1/2	$\sqrt{10} E$	$\sqrt{2} (G_x + iG_y)$	$\frac{1}{2} G_z - \frac{8}{3} D$ $+ a + \frac{2}{3} F$	$\frac{3}{2} (G_x - iG_y)$	$3\sqrt{2} E$	0
-1/2	0	$3\sqrt{2} E$	$\frac{3}{2} (G_x + iG_y)$	$-\frac{1}{2} G - \frac{8}{3} D$ $a + \frac{2}{3} F$	$\sqrt{2} (G_x - iG_y)$	$\sqrt{10} E$
-3/2	$\frac{\sqrt{5}}{2} a$	0	$3\sqrt{2} E$	$\sqrt{2} (G_x + iG_y)$	$-\frac{3}{2} G - \frac{2}{3} D$ $-\frac{3}{2} a - F$	$\frac{\sqrt{5}}{2} (G_x - iG_y)$
-5/2	0	$\frac{\sqrt{5}}{2} a$	0	$\sqrt{10} E$	$\frac{\sqrt{5}}{2} (G_x + iG_y)$	$-\frac{5}{2} G_z + \frac{10}{3} D$ $+\frac{1}{2} a + \frac{F}{3}$

TABLE 5.1 Energy Matrix for Fe/TiO₂

Note that $G_1 = g\beta H_1$.

If the Energy Matrix is \underline{E} , Eigenvalues λ are given by $|\underline{E} - \lambda \underline{I}| = 0$
where \underline{I} is Identity, and Eigenvectors \underline{x} satisfy the relation $\underline{E} \underline{x} = \lambda \underline{x}$

5.3 LINE BROADENING

A spin system can lose energy by spin-lattice interactions to maintain equilibrium after absorbing microwave radiation. The process has a characteristic relaxation time T_1 , the spin lattice relaxation time. Now from the Uncertainty Principle

$$\Delta E \Delta t \approx \hbar \quad (5.33)$$

$$\Delta E = h\Delta\nu = g \beta \Delta H \quad (5.34)$$

$$\Delta E T_1 = h\Delta\nu T_1 = g \beta \Delta H T_1 \approx \hbar \quad (5.35)$$

$$\rightarrow \Delta\nu \approx \frac{1}{2\pi T_1} \quad (5.36)$$

$$\Delta H \approx \frac{h}{g\beta} \frac{1}{2\pi T_1} \quad (5.37)$$

Another source of broadening is the exchange interaction. This results from Coulomb interactions between the electrons and from the Pauli exclusion principle which forces the same energy levels in identical ions to have a slight spread. These two processes give a single crystal lineshape characterized by a normalized Lorentzian function :-

$$F_L(H-H') = \frac{\sigma_L}{2} \frac{1}{(H-H')^2 + \frac{1}{4} \frac{\sigma_L^2}{L}} \quad (5.38)$$

where H_0 is the field at maximum absorption and σ_L is the width of the absorption line at half the maximum intensity, and the peak to peak width of the derivative line is $\sigma_L/\sqrt{3}$. A third mechanism is the spin-spin or dipolar broadening which is a result of local variations of magnetic field due to individual dipole fields. The lineshape associated with this is

the normalized Gaussian function $F_G(H)$

$$F_G(H_0 - H) = \frac{1}{\sqrt{2\pi}} \cdot \frac{1}{\sigma_G} \exp \left[-\frac{(H_0 - H)^2}{2 \sigma_G^2} \right] \quad (5.39)$$

where σ_G is the half-width of the absorption line at maximum slope, i.e. the peak to peak width of the derivative line shape is $2 \sigma_G$.

Relating the dipolar process to a relaxation time T_2 we have

$$\sigma_L = \frac{h}{g\beta} \cdot \frac{1}{\pi T_1} \quad (5.40)$$

$$\sigma_G = \frac{h}{g\beta} \cdot \frac{1.254}{2\pi T_2} \quad (5.41)$$

When both processes are present the resultant linewidth is somewhere between the square root of the sum of the individual linewidths and their sum. In this case the resultant line shape is, if σ_L and σ_G are independent of orientation, the convolution of the individual line-shapes. The convolution of a Gaussian with a Lorentzian function is called a Voigt function, which has the form

$$V(\nu) = \int_{-\infty}^{\infty} F_L(t) F_G(\nu - t) dt \quad (5.42)$$

To arrive at a powder spectra with line broadening the shape function $S(H)$ is convoluted with the appropriate lineshape $F(H)$ i.e.

$$B(H) = \int_{-\infty}^{\infty} S(H) F(H - t) dt \quad (5.43)$$

where $B(H)$ is the resultant powder lineshape.

ENERGY LEVELS OF $\text{Fe}^{2+}\text{TiO}_2$

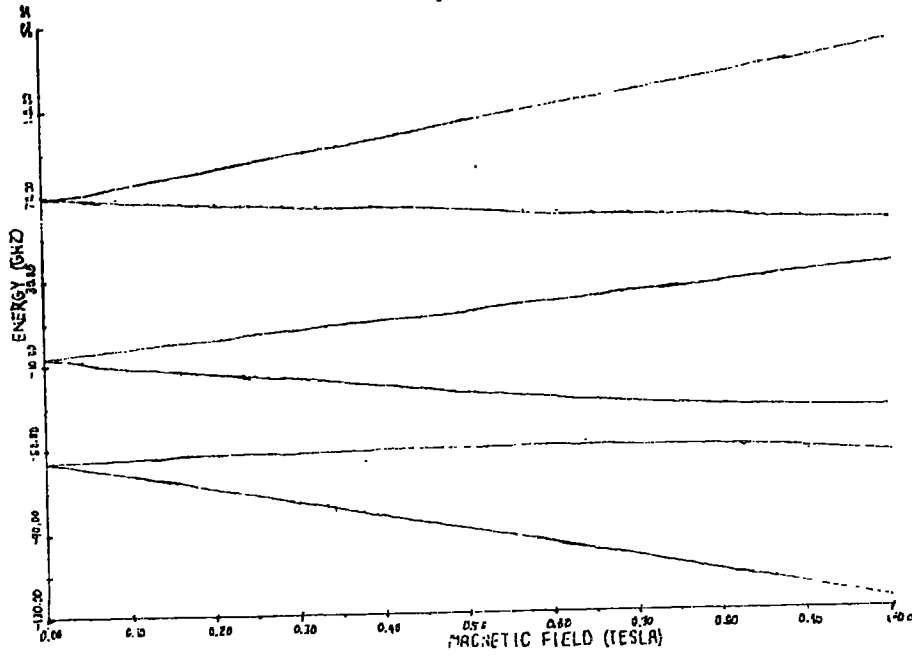


FIG 5-1

H ⊥ X AXIS.
 $\theta = 45^\circ$
 $\phi = 90^\circ$

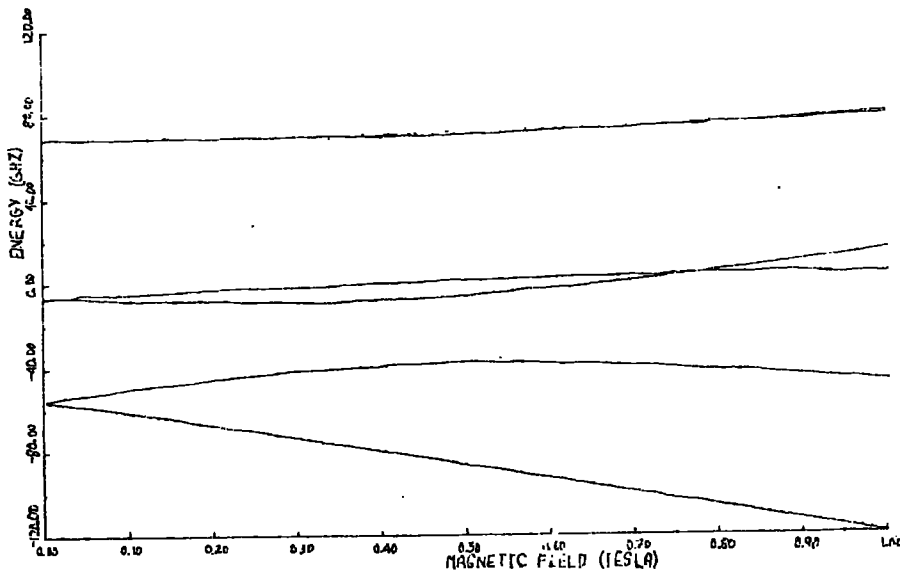


FIG 5-2

H ⊥ X AXIS
 $\theta = 45^\circ$
 $\phi = 0^\circ$

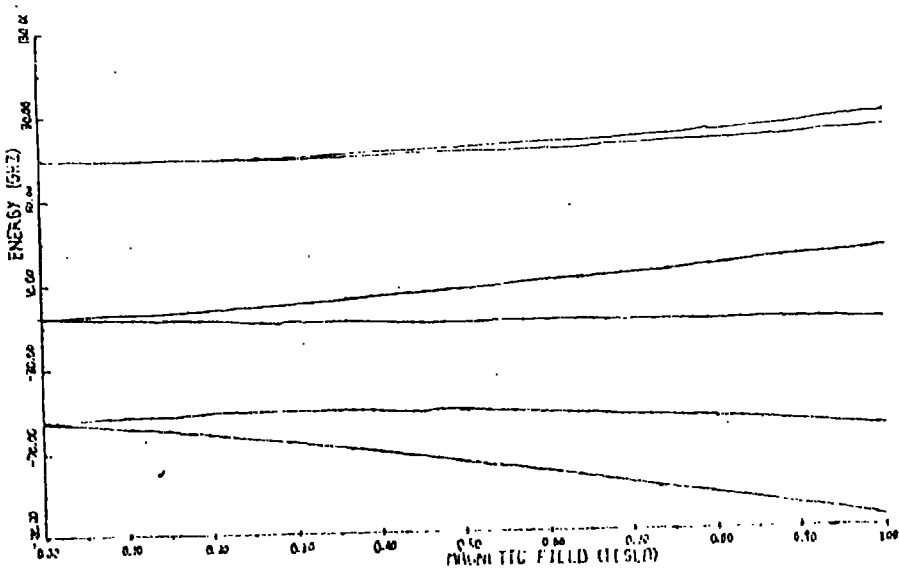


FIG 5-3

H || X AXIS
 $\theta = 0^\circ$
 $\phi = 0^\circ$

The details of the powder lineshape computation are discussed in the next chapter after alternative methods of finding the resonant field have been discussed. It took many seconds of C.P.U. time just to plot isofrequency diagrams and as calculations of the powder spectra would take much longer, different methods of finding resonant field were investigated. These are outlined below.

5.4 EVALUATION OF THE EIGENVALUES

The Energy Matrix of Table 6.1 was evaluated using numerical methods. Subroutines from the NAG (Numerical Analysis Group) subroutine library (Ref. 5.9) were used ; the exact choice of which routine to use depended on whether the eigenvalues only or the eigenvalues and eigenvectors were required. Energy level diagrams were produced simply by evaluating the energy matrix for a series of field values, (Figs. 5.1, 5.2 and 5.3).

The computation performed by the NAG subroutines starts with a similarity transformation

$$S^{-1} A S = T \quad (5.44)$$

where S is non-singular and is the product as fairly simple matrices. and T has an "easier form" than A so its eigenvectors and eigenvalues can be easily determined. The matrices A and T have the same eigenvalues and if y is an eigenvector of T then Sy is the corresponding eigenvector of A .

The form of T that is used is a tridiagonal matrix ($T_{ij} = 0$ if $|i-j| > 1$) and S is the product of $n-2$ orthogonal Householder transformation matrices (Ref. 5.12). As all eigenvalues are required they are computed from T via the QL algorithm (Ref. 5.10) and the corresponding eigenvectors of T are the product of the transformations for the QL reduction (Refs. 5.11 and 5.12).

To find the value of the resonant field with the field in a particular direction with respect to the crystallographic axes an iterative procedure was devised. However, this took a large amount of time for even a few points and so the methods detailed in the next chapter were devised.

REFERENCES

CHAPTER 5 -

- .1 P.C.Taylor, J.F.Baughner and H.M.Kriz, 'Magnetic Resonance in Polycrystalline Solids', Chem.Rev. 75 (1975) 203.
- 5.2 F.K.Kneubuhl, 'Lineshapes of E.P.R. Signals Produced by Powders, Glasses and Viscose Liquids', J. Chem.Phys. 33 (1960),1074.
- 5.3 J.S.Thorp and W.Hutton, 'Interim Report on Computer Simulation of E.S.R. Spectra', University of Durham (unpublished).
- 5.4 L.I.Schiff, 'Quantum Mechanics', (McGraw-Hill Book Co.N.Y. 1955) Ch. VI and VIII.
- 5.5 J.H.Mackey, M.Kopp, E.C.Tyman, Teh Fu Yen, 'Computer Synthesis of Electron Paramagnetic Resonances Spectra from a Parametric (Spin) Hamiltonian', Electron Spin Resonance of Metal Complexes, ed. Tek Fu Yen.
- 5.6 R.D.Dowsing and J.F.Gibson, 'E.S.R. of High Spin d^5 Systems' J.Chem. Phys. 50 (1969) 294.
- 5.7 R. Aasa, 'Powder Lineshapes in the E.P.R. Spectra of High Spin Ferric Complexes', J.Chem. Phys. 52 (1970) 3919.
- 5.8 R.H.Dicke and J.P. Wittke, 'Introduction to Quantum Mechanics' (1961) Addison Wesley.
- 5.9 N.A.G. Fortran Manual Mark. 7. (1979)
- 5.10 G. Peters, 'NPL Algorithms Library' Document No.F1/04/A.
- 5.11 J.H.Wilkinson and C. Reinsch, 'Handbook for Automatic Computation Vol. II Linear Algebra', pub. Springer-Verlag (1971).
- 5.12 J.H.Wilkinson, 'The Algebraic Eigenvalue Problem' Pub. Clarendon Press, (1965).
- 5.13 R. Aasa, T. Vanngard, 'E.P.R. Signal Intensity and Powder Shapes , A Re-examination', J. Magn. Reson. 19 (1975) 308.
- 5.14 A. Abraham, B. Bleaney, 'Electron Spin Resonance of Transition Metal Ions', Clarendon Press (1970).

- 5.15 J.C. Conesa, J. Sarice, 'Lineshapes of Powder EPR Spectra with large anisotropy : Ca II ions in Y Zeolite'
J. Magn. Reson. 33 (1979) 295.
- 5.16 J.R. Polbrow, 'Effective g Values for $S = \frac{3}{2}$ and $S = \frac{5}{2}$ '
J. Magn. Reson. 31 (1978) 479.

CHAPTER SIX

APPROXIMATE CALCULATIONS OF Fe³⁺/TiO₂ POWDER SPECTRA

The full simulation of the powder spectra detailed in the previous chapter is extremely lengthy and expensive in terms of computer time. Two different approximations were considered, both relying on treating the two observed transitions as totally separate with large anisotropic 'g' tensors and with other terms small enough to be ignored. The two methods produced the observed spectra with the exception of the relative amplitudes of the features. The first a numerical approach produced better answers but required more computer time than the second, analytical method.

These two methods both give a simplified method of solving the resonance condition :

$$h\nu = f(H)$$

and so finding the absorption spectra of the powder as before.

6.1 INTRODUCTION

Several authors (Refs. 6.1,6.2,6.3,6.4) have described the behaviour of Fe³⁺ ions in low fields by three effective g values,

g_x , g_y and g_z , for transitions within each Kramers doublet. They

used a Spin Hamiltonian of the form :-

$$H = \beta \underline{H} \cdot \underline{g} \cdot \underline{S} + D \left[S_z^2 - \frac{1}{3} S(S+1) \right] + E(S_x^2 - S_y^2) \quad (6.1)$$

to calculate the behaviour of the effective g values as a function of

λ , the ratio E/D. Wickman et al have shown that $0 \leq \lambda \leq \frac{1}{3}$. The terms

D and E are chosen so that $D > E$ and if $\frac{1}{3} < \lambda \leq 1$ simply by exchanging y and z axis gives (Ref. 6.7) :

$$\lambda_z = \frac{1 - |\lambda_y|}{1 + 3|\lambda_y|}$$

Troup and Hutton (Ref. 6.2) and Wickman et al (Ref. 6.4) have published plots of g' against λ for each transition ($\pm \frac{1}{2}, \pm \frac{3}{2}$ and $\pm \frac{5}{2}$) along the three principle axes For Fe^{3+}/TiO_2 $\lambda = 0.109$ and the observed values are compared with the values from these papers below.

	$g_x(\frac{1}{2})$	$g_y(\frac{1}{2})$	$g_z(\frac{1}{2})$	$g_x(\frac{3}{2})$	$g_y(\frac{3}{2})$	$g_z(\frac{3}{2})$	$g_x(\frac{5}{2})$	$g_y(\frac{5}{2})$	$g_z(\frac{5}{2})$
Observed effective g value	1.6	8.2	3.5	5.6	-	2.6	-	-	-
Value predicted by Troup & Hutton (Ref.6.2)	1.6	8.1	3.6	5.7	2.1	2.3	0.1	0.1	9.9

(Note: in Troup and Hutton's paper the x and z axis are interchanged, the result of selecting a different convention for the axis. The table above shows the figures in the convention used in this thesis).

There is good agreement except the $g_y(\frac{3}{2})$ term which shows the need to include higher order terms in the Hamiltonian. The $g_x(\frac{5}{2})$ and $g_y(\frac{5}{2})$ have very low values which would correspond to a field of about 6.5 Tesla which is not a low field and the approximations will not hold for this transition. To find the angular variation of the effective g values a perturbation approach should be used but as can be seen from Figs. 3.1 and 3.2 the levels diverge almost linearly in the region 0 to 0.5 Tesla. This means that the fine structure terms have a small effect on the

observed levels and the two transitions are independent of one another. Therefore we can treat the site as being composed of two independent systems, each with a 'pseudo-spin' of $S = \frac{1}{2}$. The $\pm \frac{5}{2}$ transition is not observed in the single crystal so it can be ignored. This gives rise to two Spin Hamiltonians of the form :

$$= \underline{S} \cdot g(a)_i \cdot \underline{H} \quad (6.2)$$

where a can take values $\frac{1}{2}$ and $\frac{3}{2}$ corresponding to the $\pm \frac{1}{2}$ and $\pm \frac{3}{2}$ transition respectively, and higher order terms have been ignored.

There are three principle g values g_x, g_y, g_z which can be determined empirically or deduced from the full Spin Hamiltonian. As the Spin Hamiltonian parameters are fitted to experimental results there is no particular advantage in solving the Hamiltonian rather than taking the experimental results. Equation 6.2 leads to an angular variation of the resonance field as follows :

Equation 6.2 can be rewritten as (Ref. 6.8, 6.9).

$$\mathcal{H} = \sum_k H'_k g'_k S'_k \quad (6.3)$$

for a lattice fixed coordinate system and

$$\mathcal{H} = \sum_k \sum_e H_k G_{ke} S_e \quad (6.4)$$

for a space fixed coordinate system.

where H_k, H'_k are components of the magnetic field

S'_k, S_e are components of the Pauli Spin Operator

G_k is the orientation dependent g tensor and g_k are the principle g values.

$$\text{If we take } H_k = (0, 0, H_z) \text{ and} \quad (6.5)$$

$$g = \frac{h}{H_z} \quad (6.6)$$

$$\text{we find } g^2 = g_x^2 \sin^2 \theta \sin^2 \phi + g_y^2 \sin^2 \theta \cos^2 \phi + g_z^2 \cos^2 \theta \quad (6.7)$$

6.2 NUMERICAL APPROACH

Equation 6.7 contains the angular variation of the observed single crystal lines. In Figure 6.1 the continuous curves are the observed lines and the dotted curves the angular variation predicted by equation 6.7, using the values below :-

TABLE 6.1 "g" values

	$\pm \frac{1}{2}$	$\pm \frac{3}{2}$
g_x	1.571	5.64
g_y	8.18	1.0
g_z	3.465	2.564

All the figures are from the experimental results except g_y for the $\pm \frac{3}{2}$ transition. As stated in sections 3 and 5 no resonance could be observed along the y axis. In fact at higher fields the $\pm \frac{3}{2}$ lines separate and move away from the 001 axis. The dotted curves would meet at a field of .647 tesla. This does not matter as we are only concerned with the region up to .5 T. Varying the value of g_y used in the equation gave little change to the resultant powder spectra, so this rather arbitrary choice was in fact a good approximation to the spectra.

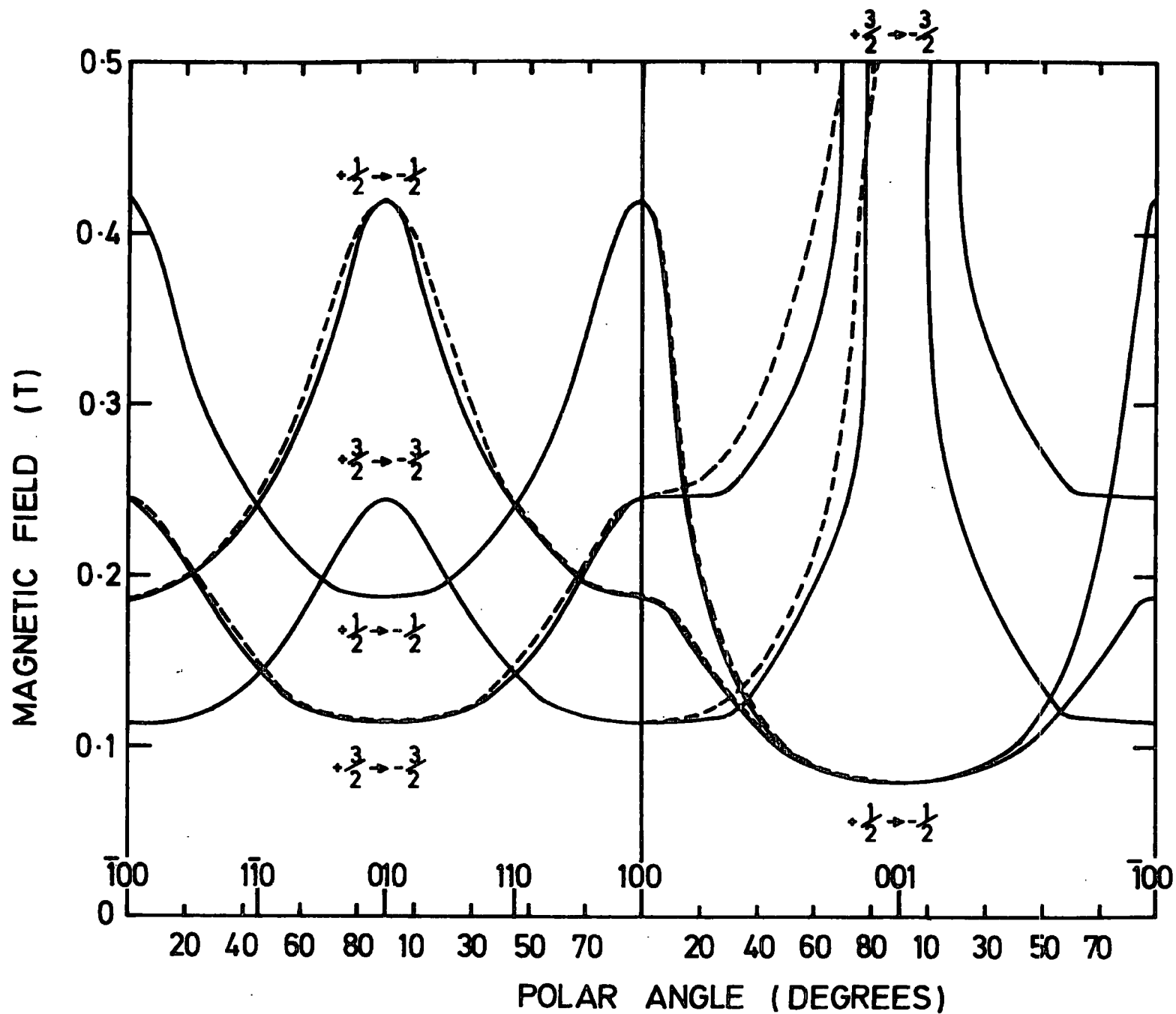


FIG. 6.1 ISOFREQUENCY PLOT FOR $\text{Fe}^{3+}/\text{TiO}_2$; 9.096 GHz. (solid line, experimental; dotted line, calculated)

6.3 ANALYTICAL APPROACH

(due to Kneubuhl, Ref. 6.8 - also Ref. 6.9)

Starting with equation (5.5) :-

$$S(H) = \Omega^{-1} (dH)^{-1} \int_{H_z}^{H_z + dH_z} d\Omega \quad (6.8)$$

we can write :-

$$S(H) = \Omega^{-1} \int_{\Omega^*} \frac{d\Omega}{|\text{grad}_{\Omega} H|} \quad (6.9)$$

where Ω^* is Ω reduced by the condition $H = \text{constant}$. As $d\Omega = d\mu d\phi$ this becomes :-

$$S(H) = \Omega^{-1} \int_{\Omega^*} \frac{1}{\text{grad } H} d\mu d\phi \quad (6.10)$$

$$= \Omega^{-1} \int_{\Omega^*} \left[\frac{\partial H}{\partial \phi} (\mu, H) \right]^{-1} \quad (6.11)$$

$$= \frac{2}{\pi} \int \left(\frac{\partial H}{\partial \phi} \right)^{-1} \sin\theta d\theta \quad (6.12)$$

Due to the symmetry of g (eqn. 6.7) we need only consider an element of

$\Omega = \pi/2$. Now from equations 6.6 and 6.7 we can write :-

$$H = \frac{h\nu}{\beta} (g_1^2 \sin^2\theta \sin^2\phi + g_2^2 \sin^2\theta \cos^2\phi + g_3^2 \cos^2\theta)^{-\frac{1}{2}} \quad (6.13)$$

where the condition $g_3 > g_2 > g_1$ must be imposed.

and writing $H_1 = \frac{h}{g_1}$ etc.

we get

$$H = (H_1^{-2} \sin^2 \theta \sin^2 \phi + H_2^{-2} \sin^2 \theta \cos^2 \phi + H_3^{-2} \cos^2 \theta)^{-\frac{1}{2}} \quad (6.14)$$

and substituting into (6.31)

$$S(H) = \frac{2}{\pi} \int_{\Omega'} \left[\frac{\partial}{\partial \theta} (H_1^{-2} \sin^2 \theta \sin^2 \phi + H_2^{-2} \sin^2 \theta \cos^2 \phi + H_3^{-2} \cos^2 \theta)^{-\frac{1}{2}} \right]^{-1} \sin \theta d\theta \quad (6.15)$$

$$= \frac{2}{\pi} \int_{\Omega'} \frac{(H_1^{-2} \sin^2 \theta \sin^2 \phi + H_2^{-2} \sin^2 \theta \cos^2 \phi + H_3^{-2} \cos^2 \theta)^{3/2}}{(H_1^{-2} - H_2^{-2}) \sin \theta \sin \phi \cos \phi} d\theta \quad (6.16)$$

Evaluating the integral we find that

$$H_1 < H < H_2$$

$$S(H) = \frac{2}{\pi} \frac{H_1 H_2 H_3 H^{-2}}{(H_1^2 - H^2)^{\frac{1}{2}} (H_2^2 - H_3^2)^{\frac{1}{2}}} K(k) \quad (6.17)$$

$$H_3 > H > H_2$$

$$S(H) = \frac{2}{\pi} \frac{H_1 H_2 H_3 H^{-2}}{(H_1^2 - H_2^2)^{\frac{1}{2}} (H - H_3^2)^{\frac{1}{2}}} K(1/k) \quad (6.18)$$

$$\text{all other } H, S(H) = 0 \quad (6.19)$$

$$\text{where } k = \frac{(H_1^2 - H_2^2)(H^2 - H_3^2)}{(H_1^2 - H^2)(H_2^2 - H_3^2)} \quad (6.20)$$

and $K(k)$ is an elliptical integral of the first kind :

$$K(k) = \int_0^{\pi/2} \frac{db}{(1-k^2 \sin^2 b)^{1/2}}$$

$$= \left(1 + \left(\frac{1}{2}\right)^2 k^2 + \left(\frac{1 \cdot 3}{2 \cdot 4}\right)^2 k^4 + \left(\frac{1 \cdot 3 \cdot 5}{2 \cdot 4 \cdot 6}\right)^2 k^6 + \dots \right) \quad (6.21)$$

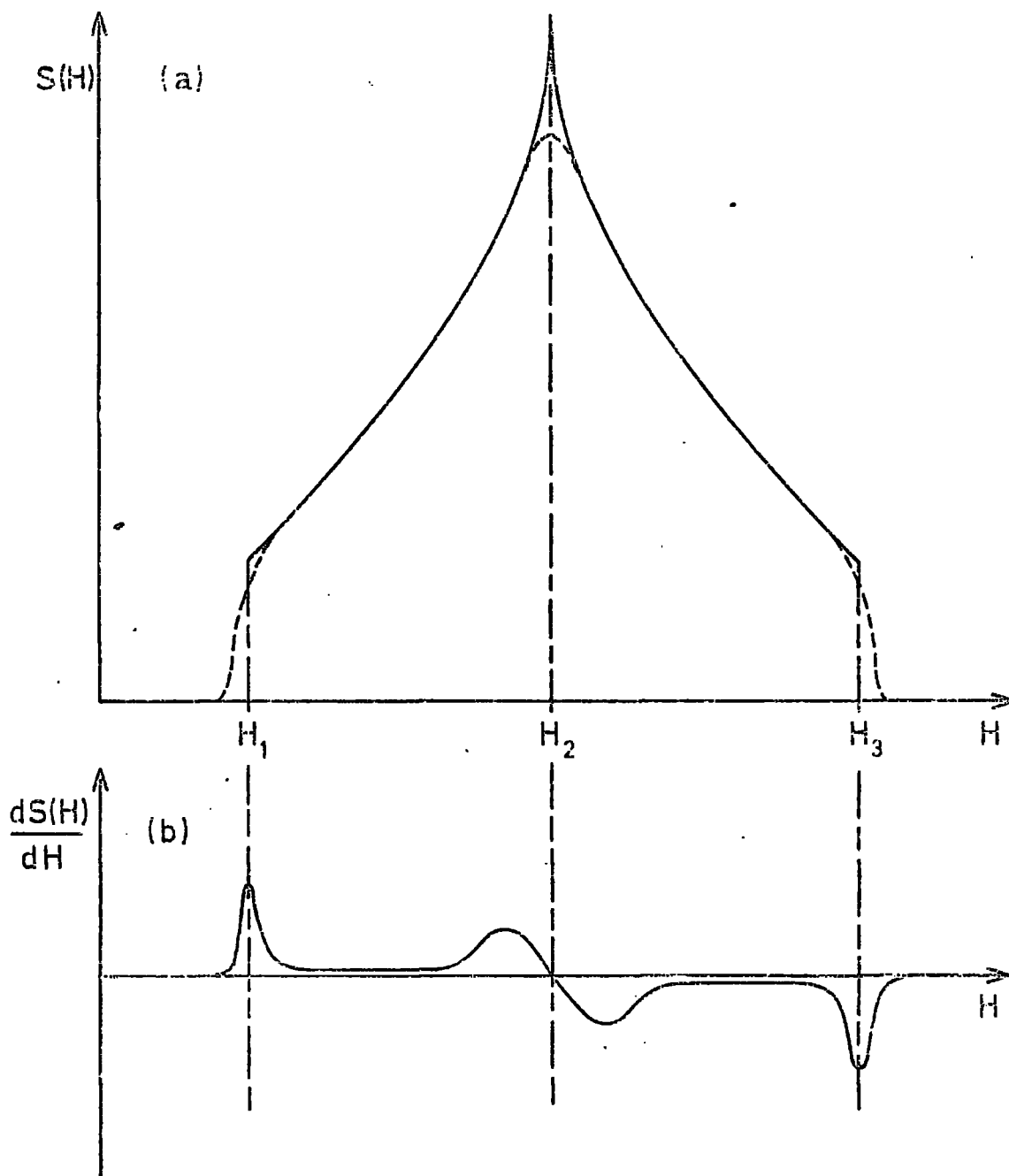
and $K(0) = \pi/2$

$K(1) = \infty$

Inspection of 6.17, 6.18 and 6.19 shows that the spectra will have singularities at $H = H_1$ and $H = H_3$. From (6.20) $H = H_2$ implies that $k = 1$ & from 6.21 $K(k) = \infty$, i.e. $S(H) = \infty$, so a third singularity at $H = H_2$ is expected. The H_1 and H_2 singularities correspond to a step and that at H_3 to a peak (Fig. 6.2a). The function $S(H)$ can be convoluted with a lineshape function for each transition in Fe/TiO_2 and the resultant lineshape function $\hat{S}(H)$ is the sum of the individual $S(H)$'s.

$$S(H) = a \frac{S_1}{2}(H) + \frac{S_3}{2}(H)$$

where a is a constant to simulate the effect of different amounts of absorption for each transition. This assumes that the transition probability is independent of the orientation of the applied magnetic field. This method has been improved to take account of varying transition probability, to obtain a similar formula, but with extra terms containing elliptical integrals of the first and second kind (Ref. 6.11).



(a) ——— LINESHAPE WITH NO LINE-BROADENING.

----- LINESHAPE WITH LINE - BROADENING.

SINGLE CRYSTAL LINEWIDTH $\sigma \ll H_2 - H_1$

AND $\sigma \ll H_3 - H_2$.

(b) DIFFERENTIATED LINESHAPE WITH $\sigma \ll H_2 - H_1$

AND $\sigma \ll H_3 - H_2$.

FIG. 6-2 THEORETICAL POWDER LINESHAPE

6. COMPUTATION

The calculation was performed on the NUMAC IBM 360/168 system in Newcastle.

To perform the integration of equation 5.3, the resonant fields for many directions of magnetic field has to be found. This is equivalent to solving an equation of the form

$$h\nu = f(H, \theta, \phi)$$

many times. In a powder the crystallites are randomly orientated and so selecting the θ and ϕ randomly would give a true simulation. However, this approach needs a lot of computer time and for a given number of orientations examined it is best to choose a regular grid of directions. These directions must be subtend equal amounts of solid angle (i.e. $\Delta\phi\Delta\theta \sin\theta$ must remain constant where $\Delta\phi$ and $\Delta\theta$ are the difference between adjacent directions). This is because the resultant spectra derived using the regular distribution of directions has less "noise" than the Monte Carlo approach (Ref. 6.10).

Due to the symmetry of the system only an integration over a $\Omega = \pi/2$ need be performed. The g value corresponding to values ϕ and $\sin\theta$ was calculated and the corresponding value of resonant field found. An array with each element $H(a)$ corresponding to a field range $H(a)$ to $H(a) + \Delta H = H(a + 1)$ was set up and the array element incremented each time that the resonant field H_r obeyed :-

$$H(a) < H_r(\phi, \sin\theta) < H(a) + \Delta H$$

This is performed for both transitions and the two resulting arrays summed. By adding different amounts to the array for each transition the effect of differing transition probabilities could be simulated. The effect noted in section 5.2 due to the field swept techniques was included by multiplying each element by $1/g$. This array represents $S(H)$ and was convoluted with

the appropriate line broadening function. As the array represents a histogram of the absorption in which each element has the same width ΔH , the differentiation could be performed simply by finding the difference between successive elements. This resultant spectra could then be compared directly with the observed powder spectra.

The output was displayed on a graphplotter using a plotting routine (written by P. Waite) and was also available as a list of the coordinates of the points.

The data in Table 6.1 was used as the basic data. The variables which could be adjusted to give a better fit between theory and experiment were

- (a) Linewidth, Sigma σ
- (b) Relative Transition Probability.

A Gaussian line broadening function was used, but because σ_G was so much smaller than the range of resonant fields, the type of function did not change the large scale appearance of the computed lineshape. Chapter 7 presents the output of this program and compares the results with the experimental spectra. This method had produced a reasonable simulation and although further investigation could produce a better fit, the features can be clearly identified. Further work should be done to be able to explain the whole spectra in detail.

As in iron doped rutile the difference in principal H values (H_1, H_2 and H_3) is large, of the order of 0.1 Tesla, and the line broadening of the single crystal lineshapes is of the order of 0.001 Tesla when the powder spectra is differentiated it gives rise to three apparently separate features. As there are two observable transitions in Fe/TiO_2 we would expect to see six features. Using the field corresponding to Table 6.1 we would only expect to see five features as one (at 0.647 tesla) is out of the field range examined.

Expected Features (in range 0-500mT)	Observed Features (mT)
79.1	A 79.55
114.8	B 115.59
186.0	C 192.35
254.2	D 248.61
412.0	E 276.33

Thus features A, B, C and D of Fig. 5.4 were identified with the Fe^{3+} ion as before. The only remaining problem is that the expected feature at 412.0 mT is not seen. This is because the absorption spectra of 6.2 is not quite accurate. The step at H_1 is in fact the largest part of the absorption spectra. This means that this step will be far larger than the step at H_3 and the feature due to H_3 will be little larger than the background noise.

Although the variation of transition probability with angle was not used in these calculations, it has been predicted by several authors (Refs. 6.12, 6.13 and 6.14) and could be included simply by incrementing the array corresponding to $S(H)$ by a number proportional to the transition probability.

REFERENCES

CHAPTER SIX -

- 6.1 J.R.Pilbrow, "Effective g Values for $S = \frac{3}{2}$ and $S = 2 \frac{5}{2}$ ",
J.Mag. Reson. 31 (1978) 479.
- 6.2 G.R.Troup and D.R. Hutton, "Paramagnetic Resonance of Fe^{3+} in
Kyanite", Brit. J. Appl. Phys. 15 (1964) 1493.
- 6.3 F.Hoby, J.R.Thyer, and N.E. Hedgecock, "E.S.R. Spectra of
 Fe^{3+} in Single Crystals of Andalusite", Can. J.Phys. 44 (1966) 509.
- 6.4 H.H.Wickman, M.P.Klein, D.A.Sherley, "Paramagnetic Resonance
of Fe^{3+} in Polycrystalline Ferrichrome A*", J.Chem.Phys. 42
(1965) 2113.
- 6.5 R.D.Dowling and J.F. Gibson, "E.S.R. of High Spin d^5 Systems"
J.Chem. Phys. 50 (1969) 294.
- 6.6 A. Ehrenberg, B.E.Malmström and T. Vangord (Eds) "Magnetic
Resonance in Biological Systems", pub. Pergamon Press Ltd.,
London 1967, see. W.E.Blumberg p.119.
- 6.7 K.D.Bowers and J.Owen,
Rep.Prog. Phys. 18 (1955) 304 (see page 321).
- 6.8 P.C.Taylor, J.F.Baughner and M.M. Kriz, "Magnetic Resonance
in Polycrystalline Solids", Chem.Rev. 75 (1975) 203.
- 6.9 F.K. Kneubuhl, "Lineshapes of EPR signals produced by Powders
Glasses and Viscous Liquids", J.Chem.Phys. 33 (1960) 1074.
- 6.10 P.C.Taylor and P.J.Bray, "Computer Simulations of Magnetic
Resonance Spectra Observed in Polycrystalline and Glassy Samples",
J.Mag.Reson. 2 (1970), 305.
- 6.11 F.K. Kneubuhl and B. Natterer, "Paramagnetic Resonance Intensity
of Anisotropic Substances and its Influence on Line Shapes",
J.Chem.Phys. 34 (1961) 710.

- 6.12 G.J.Troup and D.R.Hutton, "Paramagnetic Resonance of Fe^{3+} in Kyanite", Brit.J.Appl.Phys. 15 (1964) 1493.
- 6.13 H.H.Wickman, M.P.Klein, and D.A. Shirley, "Paramagnetic Resonance of Fe^{3+} in Polycrystalline Ferrichrome A*", J.Chem. J.Chem Phys. 42 (1965) 2113.
- 6.14 F.Hobey, "The Spin Hamiltonian and Intensities of the ESR Spectra Originating from Large Zero Field Effects of States", Can.J.Phys. 44 (1966) 503.

CHAPTER SEVEN

EXPERIMENTAL AND THEORETICAL POWDER LINESHAPES OF Fe/TiO₂

7.1 EXPERIMENTAL POWDER SPECTRA

In the single crystal specimens examined in Chapter 4 there was a large isotropic feature whose origin was not entirely clear. It would be expected that this line would be unchanged when the samples are powdered and this proved to be the case so that the observed spectra are a superposition of this wide line and spectra due to iron, nickel and the other paramagnetic ions. Much higher sensitivity measurements are required to detect the powder spectra because only a few of the ions contribute to the absorption at a particular value of the applied magnetic field. The results are summarized in Table 7.1.

7.1.1 Room Temperature

The spectrum observed in a powdered fragment of the Swiss boule is shown in Figures 7.1 to 7.5. There are five main features labelled A,B,C,D and E. Features A,B,C and D are shown in more detail in Figures 7.2 to 7.5. The pigments showed only the large isotropic feature referred to above.

7.1.2 Liquid Helium Temperatures

The powdered Swiss boule spectrum is shown in Fig. 7.6. Lines A,B,C and D are still present ; they correspond to the four lowest principle 'g' values of the iron spectra and later in this chapter these features will be related to the Fe³⁺ ion. Line E is no longer visible. Two new large lines labelled F and G can be seen as well as several smaller lines, for example, the line at 22.5 mT. The pigments did not show any spectra due to iron but did show features F and G. The latter appeared to be enhanced by optical irradiation but no

Table 7.1: Fe/TiO₂ Observed Powder Spectra with a frequency of 9.095 GHz.

Feature	Field (mT)	'g' value	Appearance	Width mT approx.
A	79.54	8.18	Spike-differentiated Step	2 mT
B	115.59	5.62		2.5 mT
C	198.35	3.378	Differentiated Peak	4 mT
D	248.51	2.614		4 mT
E	276.33	2.352	Differentiated Peak - not visible at 5 K	5 mT
F			Differentiated Peak - not visible at Room Temperature	
G			Double peak U.V. sensitive	

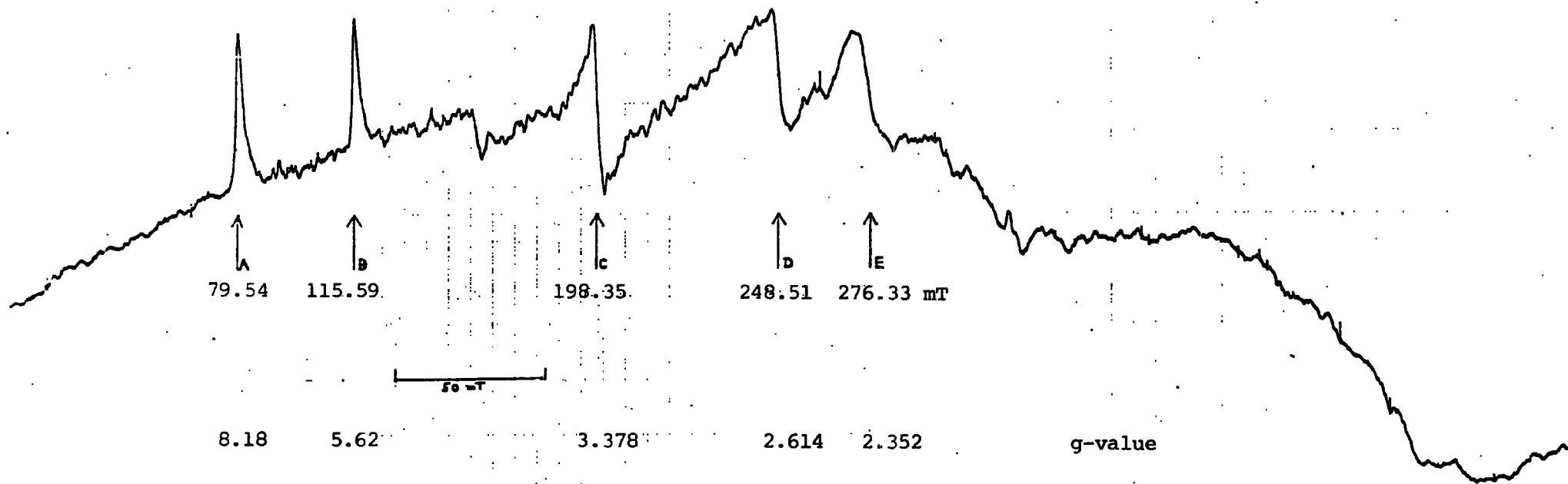
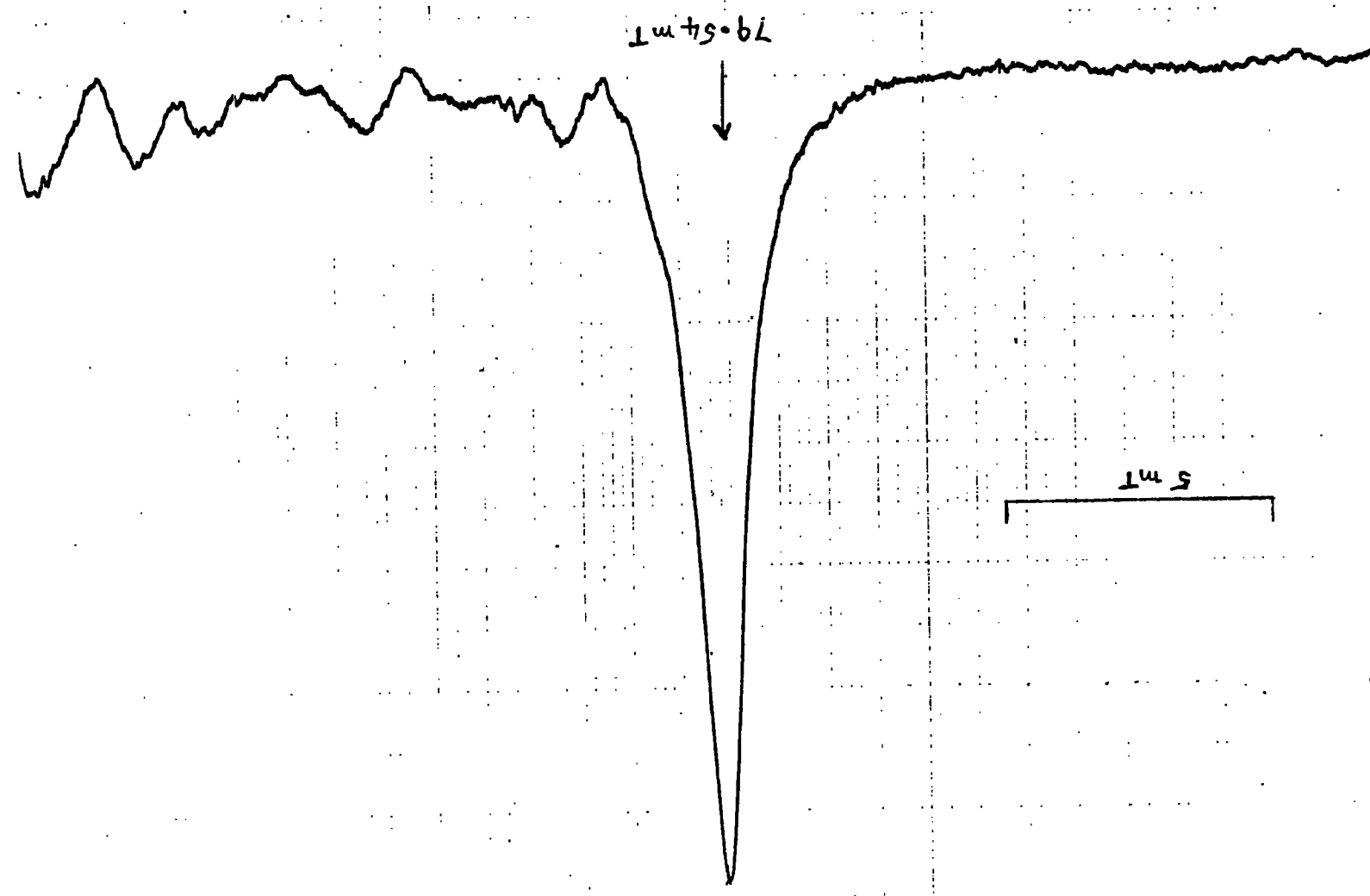


FIG. 7.1 Spectrum of powdered Fe/TiO₂, 9.095 GHz. (High Fe concentration).



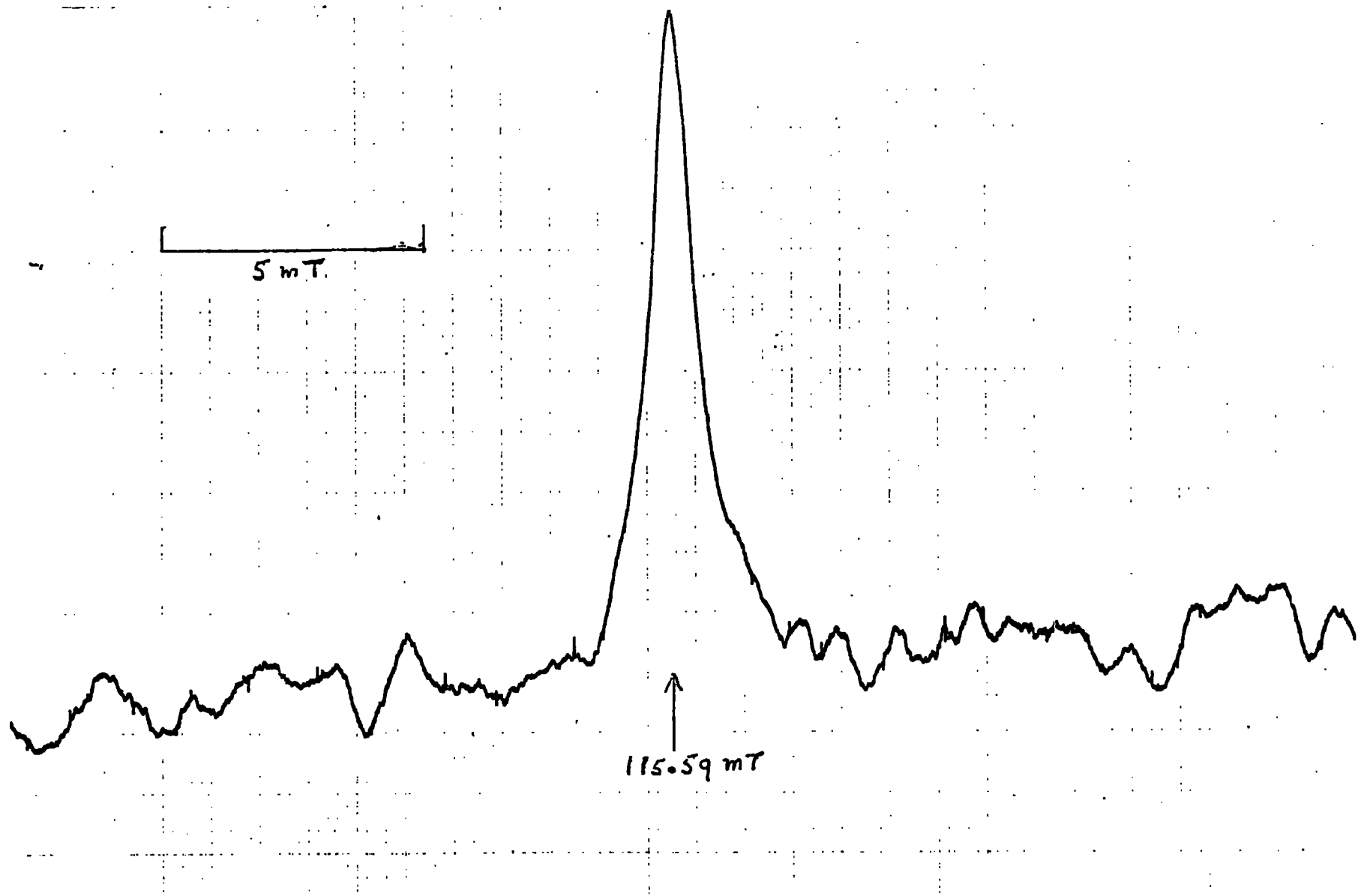


FIG. 7.3 Feature B of Fig. 7.1 ; 9.045 GHz.

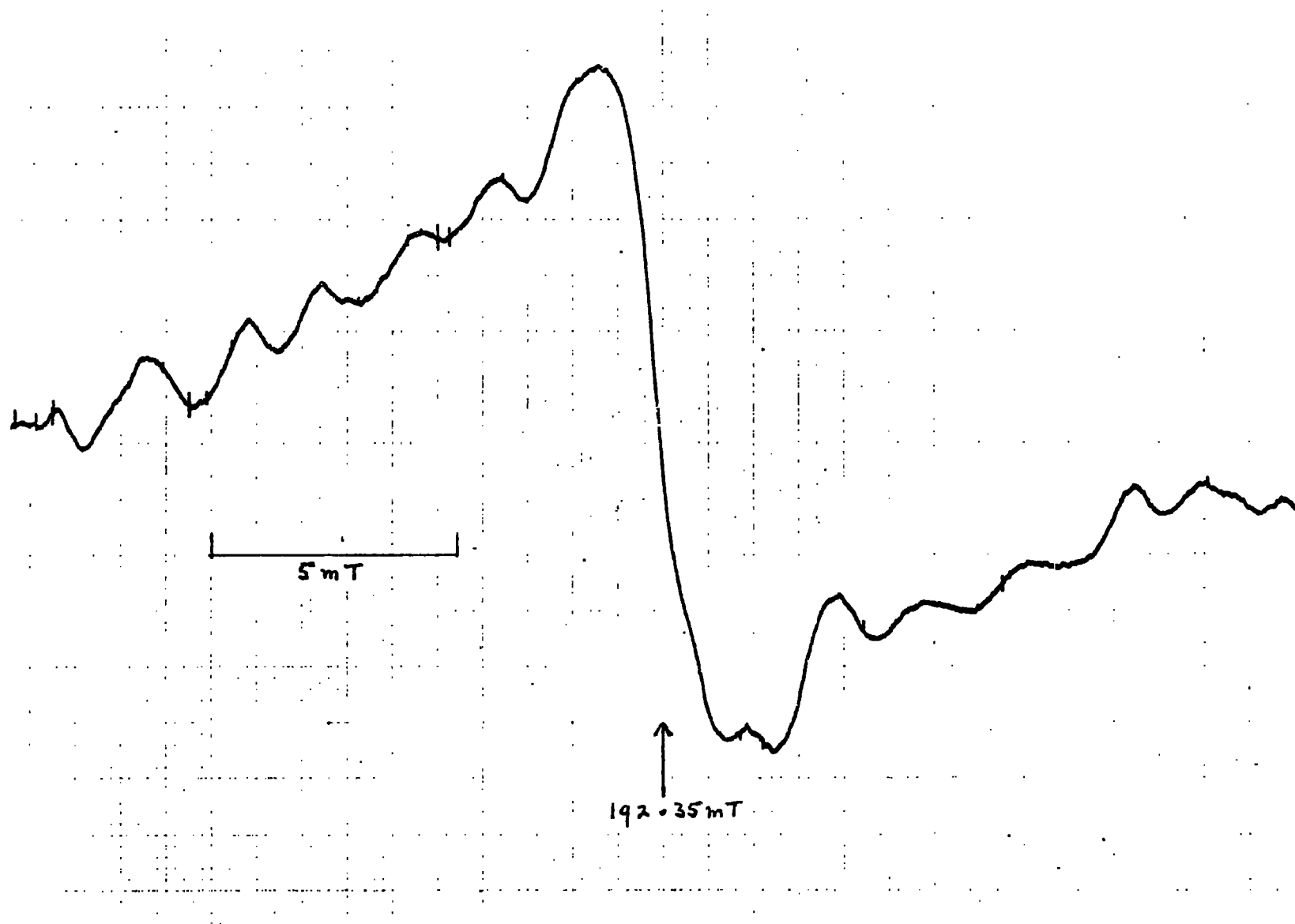


FIG. 7.4 Feature C of Fig. 7.1 ; 9.095 GHz

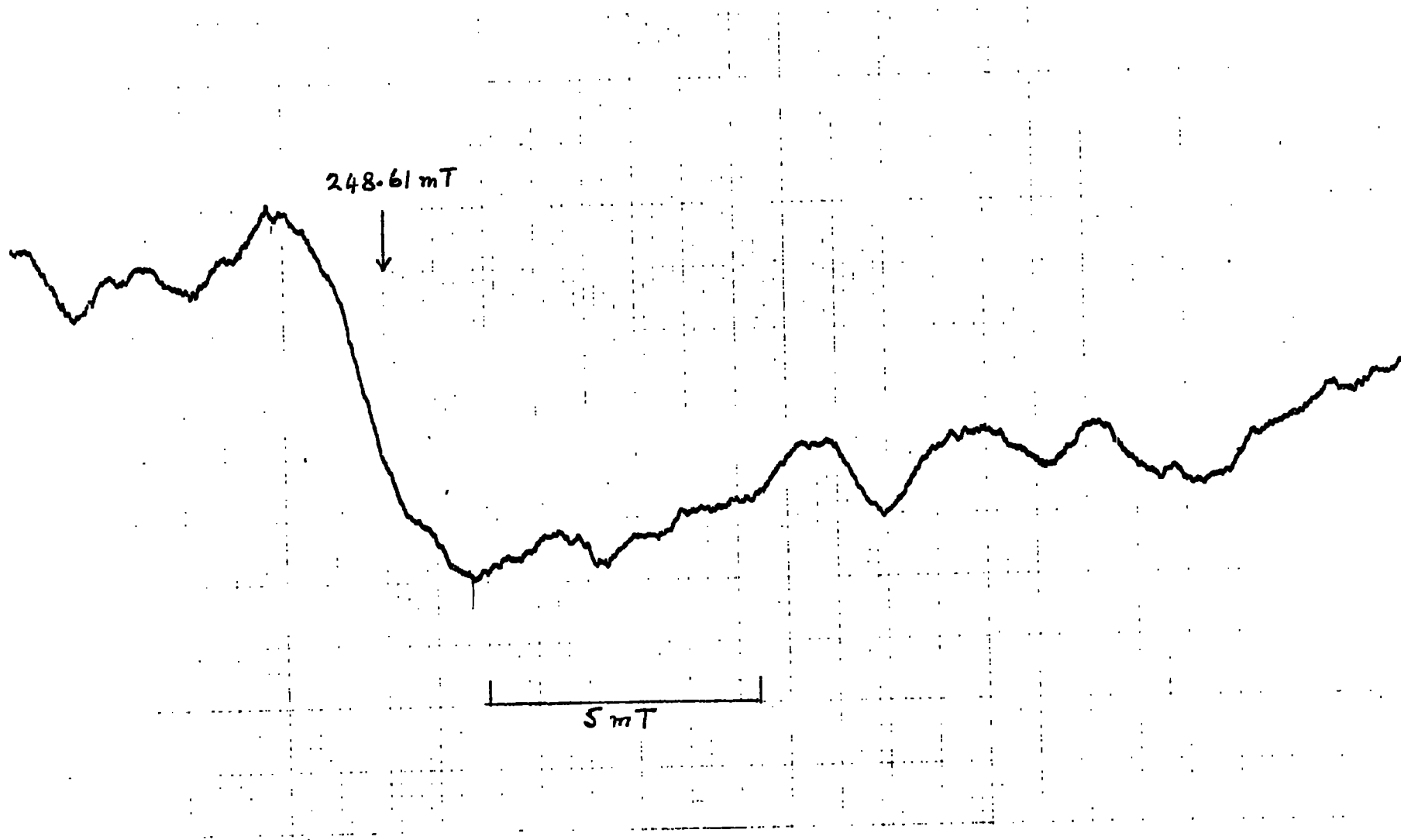
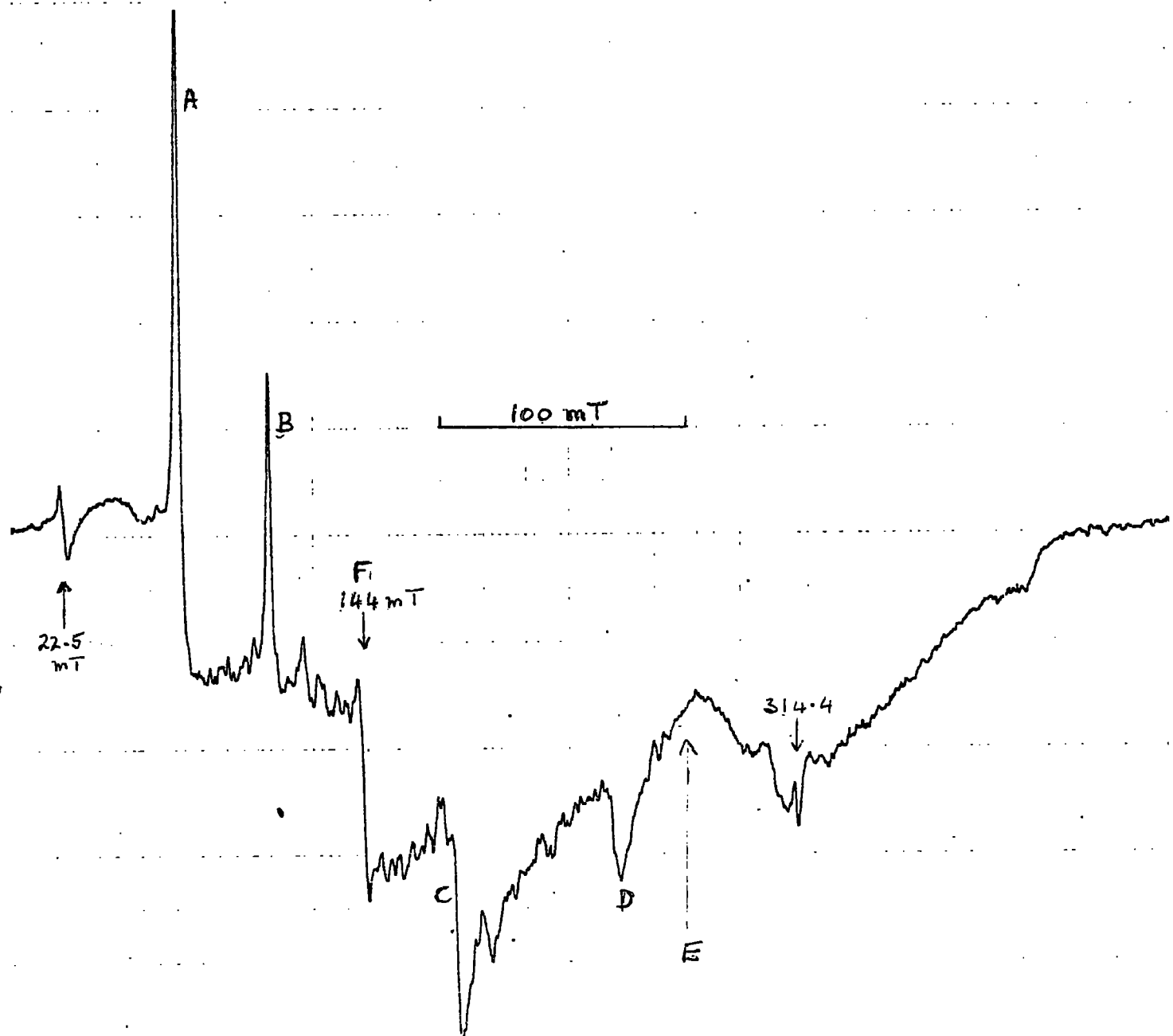


FIG. 7.5 Feature D of Fig. 7.1 ; 9.095 GHz



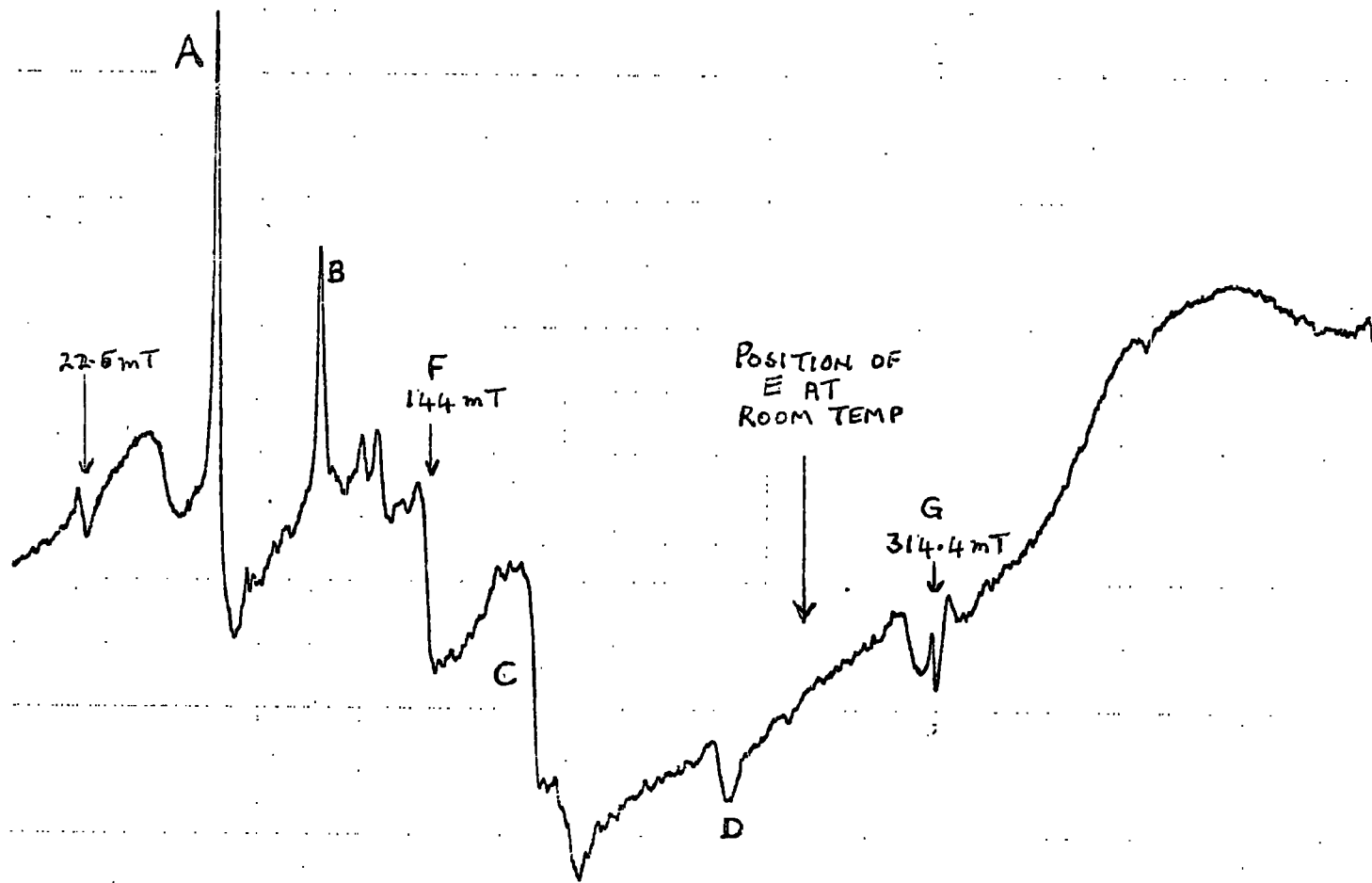


FIG 7.6 POWDER SPECTRUM OF Fe/TiO₂; 6.5K.

extensive investigation of this could be performed in the time available. The spectrum of pigment C is shown in Fig 7.7.

The relative intensities of the features A, B, C and D when compared with their intensities at room temperature are of interest. Later A and C will be shown to be due to the $\pm \frac{1}{2}$ transition of the Fe^{3+} ion and B and D to the $\pm \frac{3}{2}$ transition. It appears that the intensity of B and D compared with A and C increases as the temperature rises. Also, C and D are larger at room temperature when compared to A and B.

7.2 COMPUTED SPECTRA

These spectra do not include the effect of the wide line mentioned above or of any other ion apart from Fe^{3+} . The main interest of this thesis lies in developing techniques for identifying the Fe^{3+} spectrum in a powder specimen. This has been performed successfully. The importance of this is that the method is of general applicability so that powder spectrum features due to other ions may be predicted by simply utilising the parameters appropriate to that particular ion in the computer simulation.

7.2.1 Results of Kneubuhl's Method (Ref. 7.1)

Figure 7.8 shows the result of evaluating the equation 6.17 to 6.21 for a variety of linewidths. The two features A and B are well simulated but C and D have far too small an amplitude to give any confidence in the method. There is also a 'line' at 420 mT which is not observed. The g^{-1} factor due to Oasa and Vanngard (Ref. 7.2 and Chapter 5) was included and a comparison, between Fig 7.9 without the factor and Fig. 7.10 including g^{-1} , shows little improvement in the spectra.

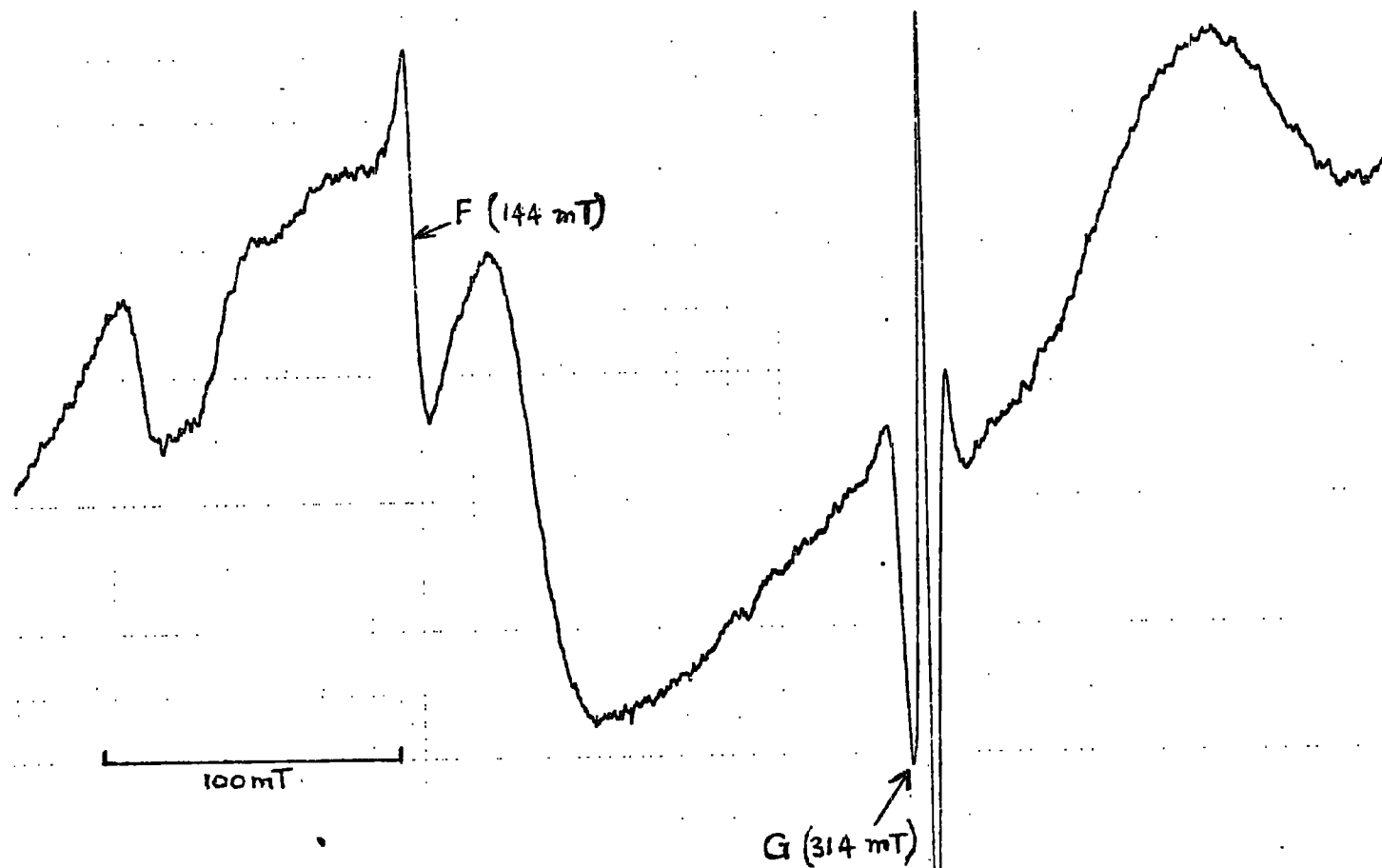


FIG 7.7. SPECTRUM OF PIGMENT C;
5.9 K.

FIG. 7.8 POWDER SPECTRA OF IRON DOPED RUTILE

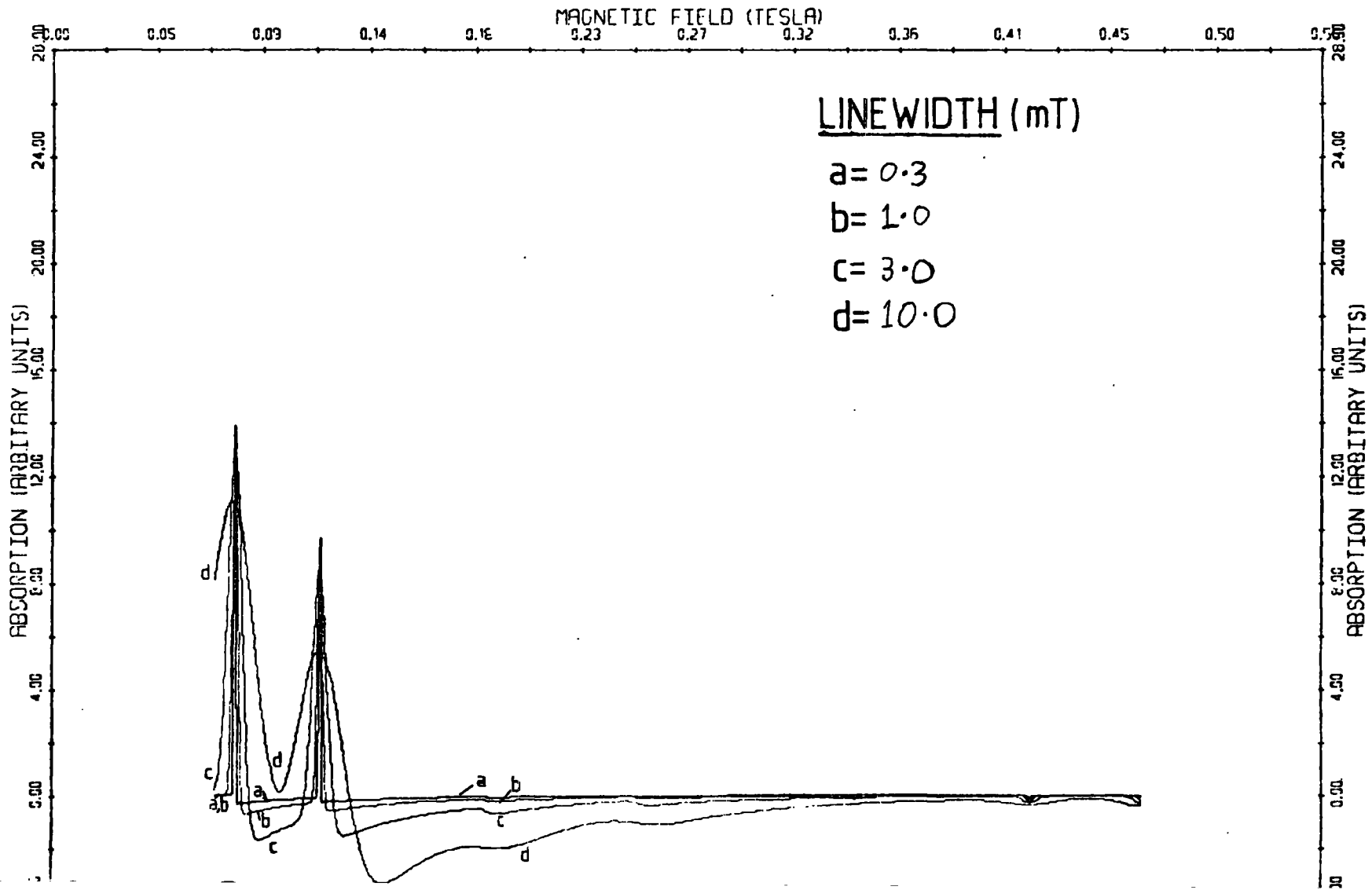


FIG. 7.9

E.S.R. POWDER LINE TiO_2/Fe^{3+}

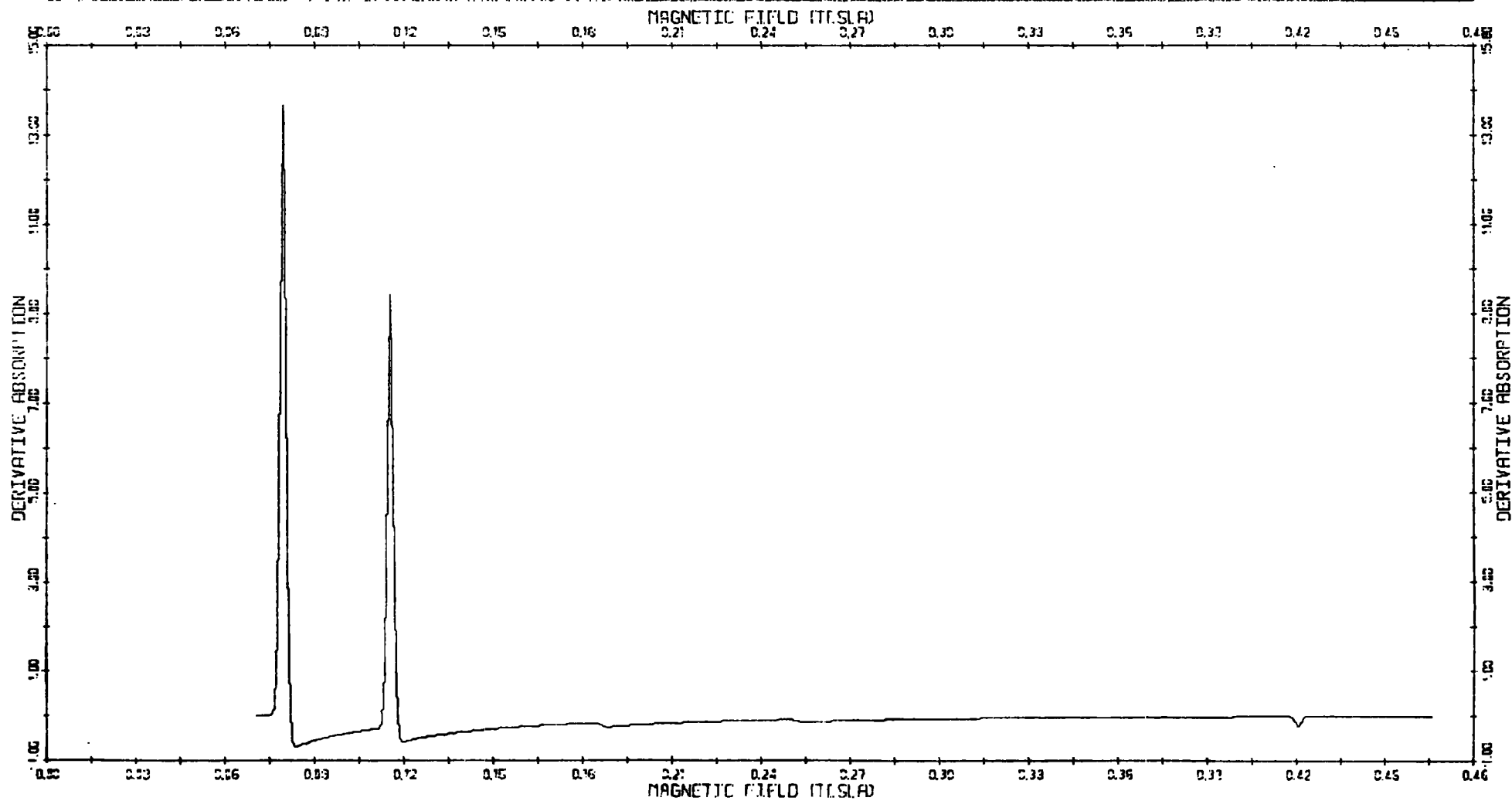
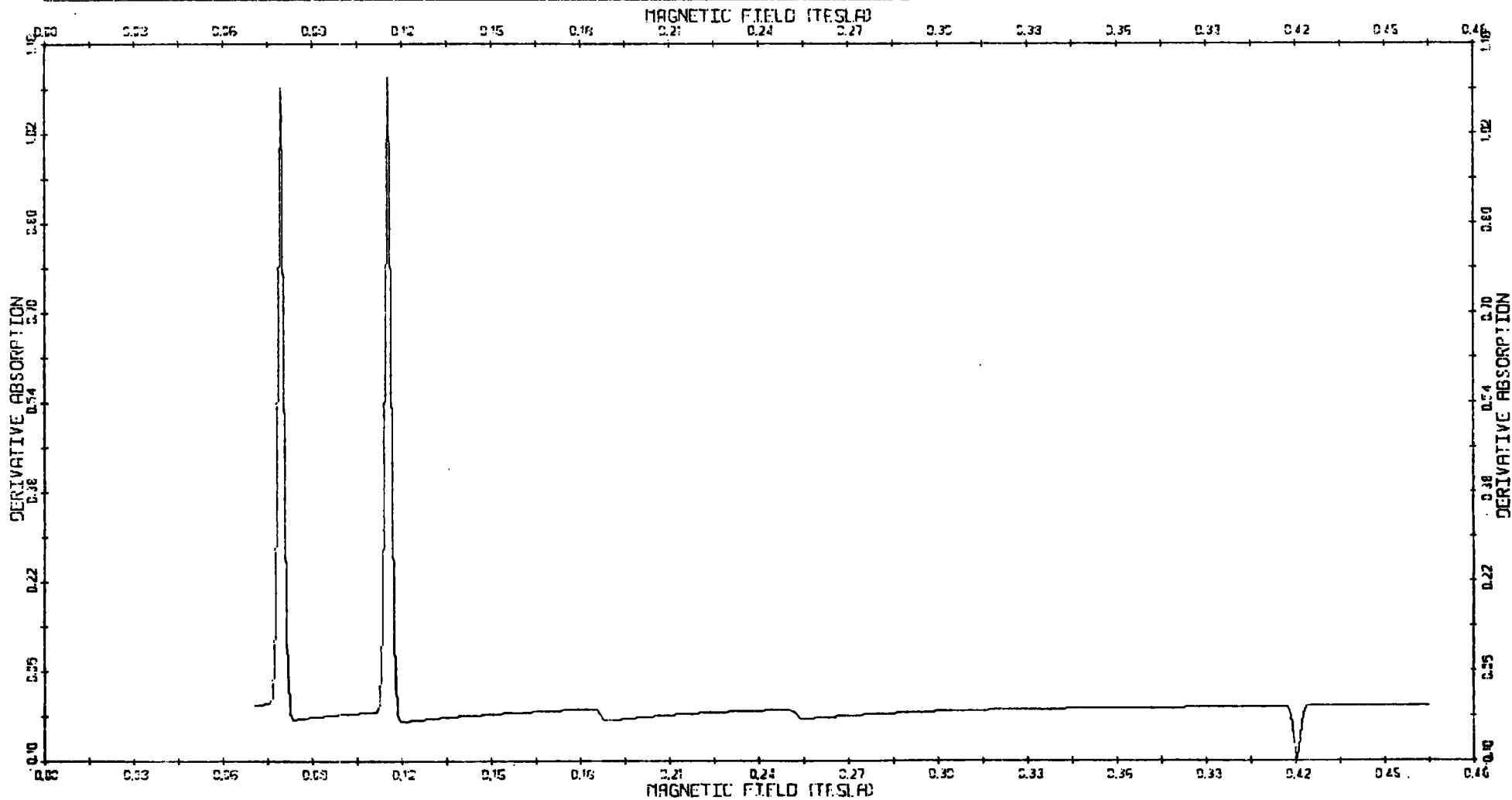


FIG. 7.10

E.S.R. POWDER LINE TiO_2/Fe^{3+}



7.2.2 Results of the Numerical Approach

The graphs, Fig.7.11 to 7.17 show the result of evaluating the numerical method described in Section 6.2 and varying some of the parameters as shown below.

Linewidth (mT)	Figure		g^{-1} factor
	$I(\frac{1}{2}) = I(\frac{3}{2})$	$I(\frac{1}{2}) = 2I(\frac{3}{2})$	
2.0	7.11	-	not included
0.1	7.12	7.15	included
1.0	7.13	7.16	included
5.0	7.14	7.17	included

TABLE 7.2 Key to results of Numerical Approach.

The four features A, B, C and D are well simulated as regards shape and position (Table 7.3). In Fig 7.11 the g^{-1} factor was not included and the amplitudes of C and D were smaller than the observed ratios. Including the g^{-1} factor gives a far better fit and Fig.7.16 gives a good simulation of the observed spectra at low temperatures (Fig. 7.6). However the amplitude of the spectra at higher temperatures is not well simulated.

7.3 CONCLUSIONS

7.3.1 Kneubuhl's Method

This did not provide adequate simulations of the observed spectra. This is most probably due to (a) computing the differential of a discontinuous function ($S(H) \rightarrow \infty$ for $H \rightarrow H_1$ or H_2 or H_3) and (b) the equation assumes that the intensity of the line is constant which it is not. Kneubuhl and Natterer (Ref. 7.3) have included the

FIG. 7.11 POWDER SPECTRA OF IRON DOPED RUTILE

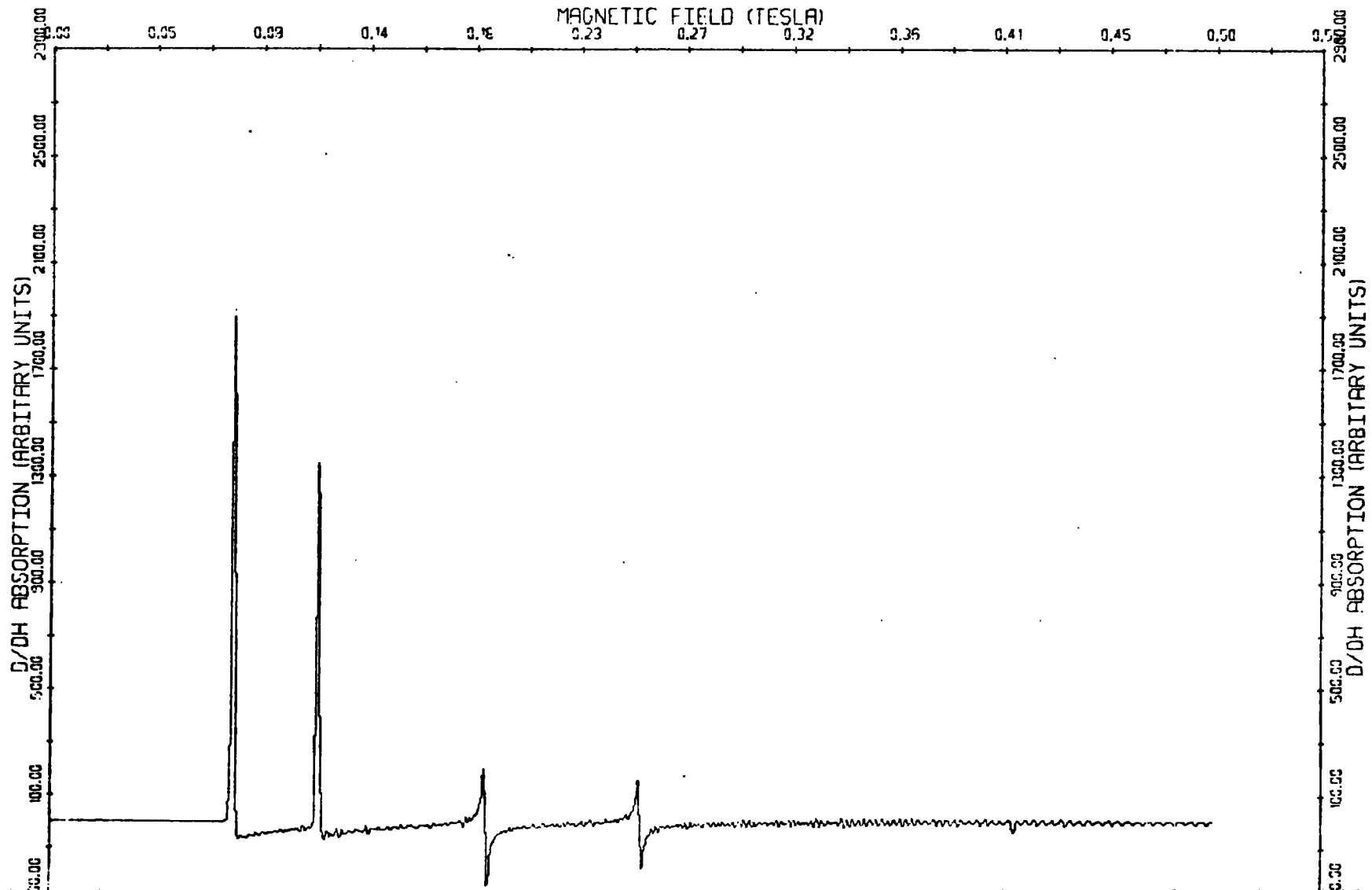


FIG. 7.12

E. S. R. POWDER LINE $\text{TiO}_2/\text{Fe}^{3+}$

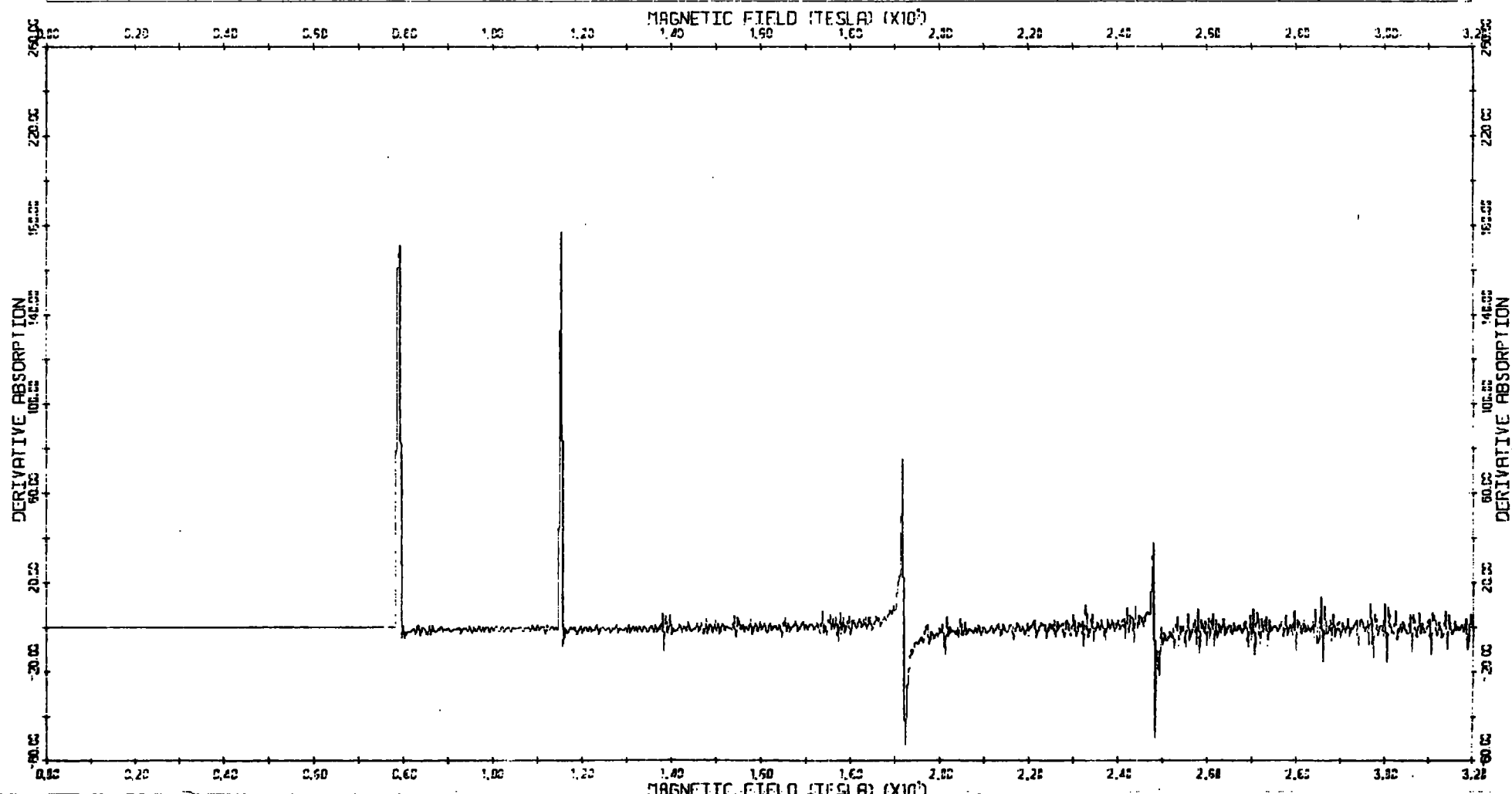


FIG 7-13

E.S.R. POWDER LINE $\text{TiO}_2/\text{Fe}^{3+}$

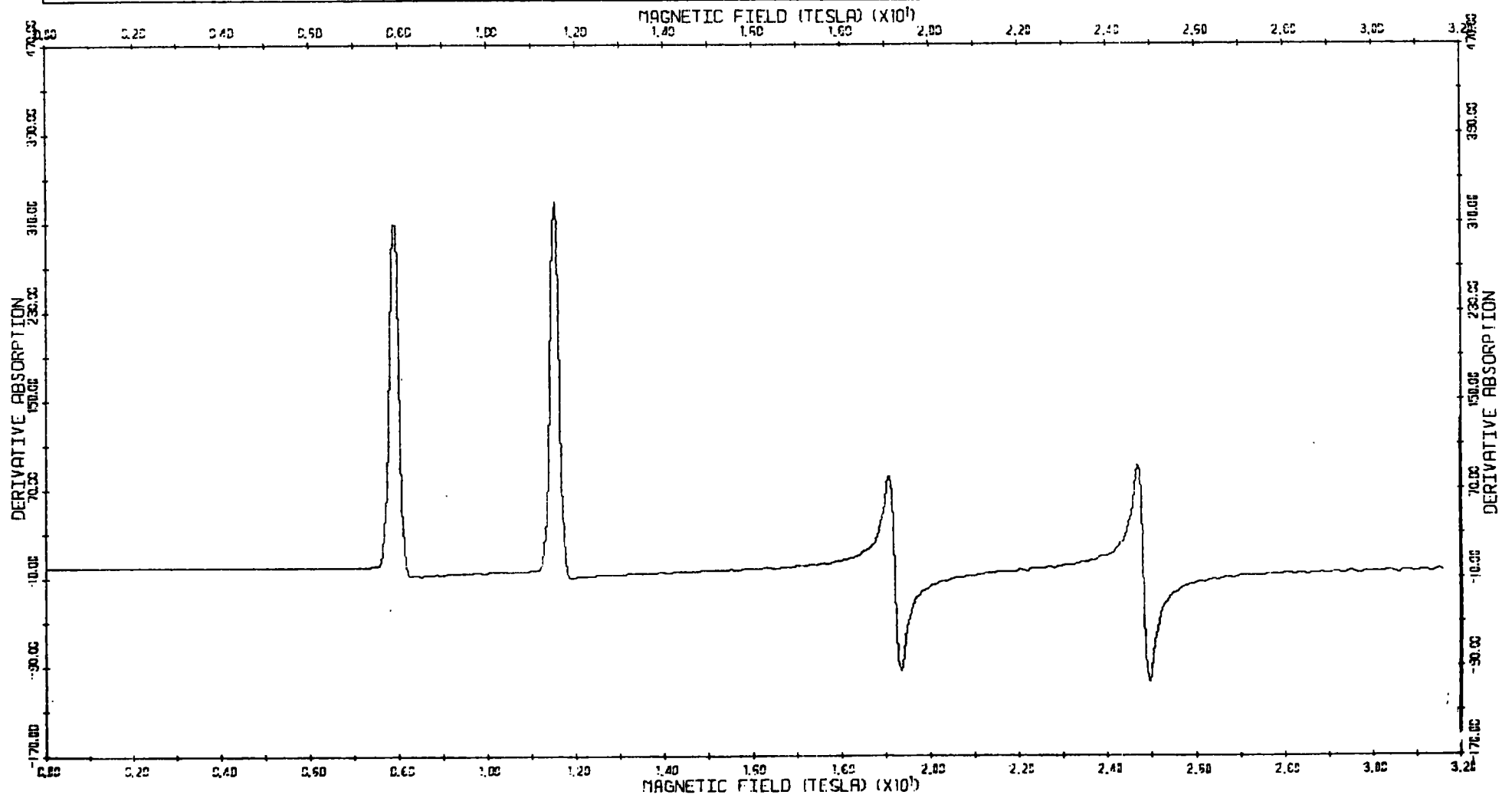


FIG. 7.14 E.S.R. POWDER LINE $\text{TiO}_2/\text{Fe}^{3+}$

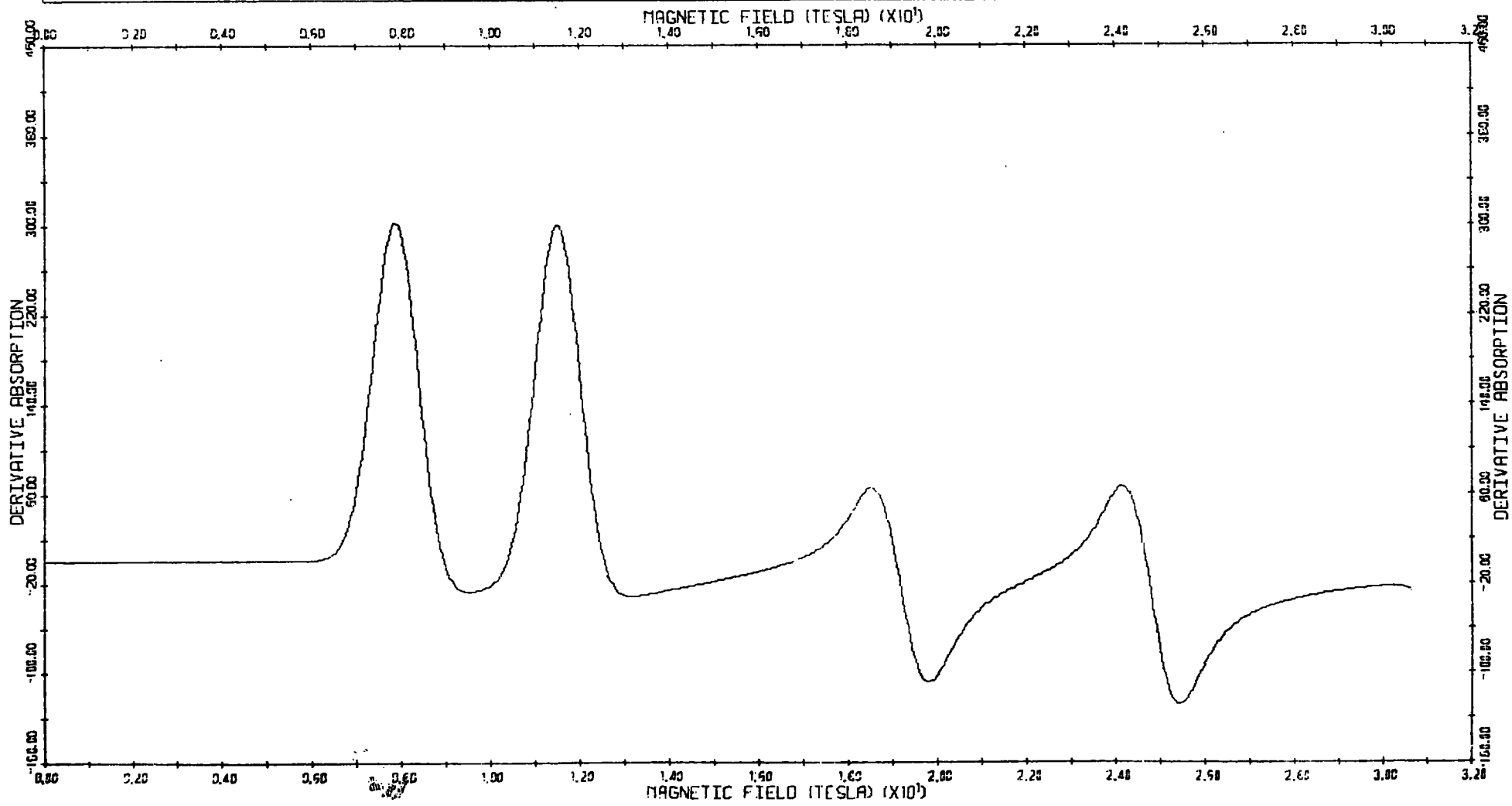


FIG 7-15

E.S.R. POWDER LINE Fe^{3+}/TiO_2

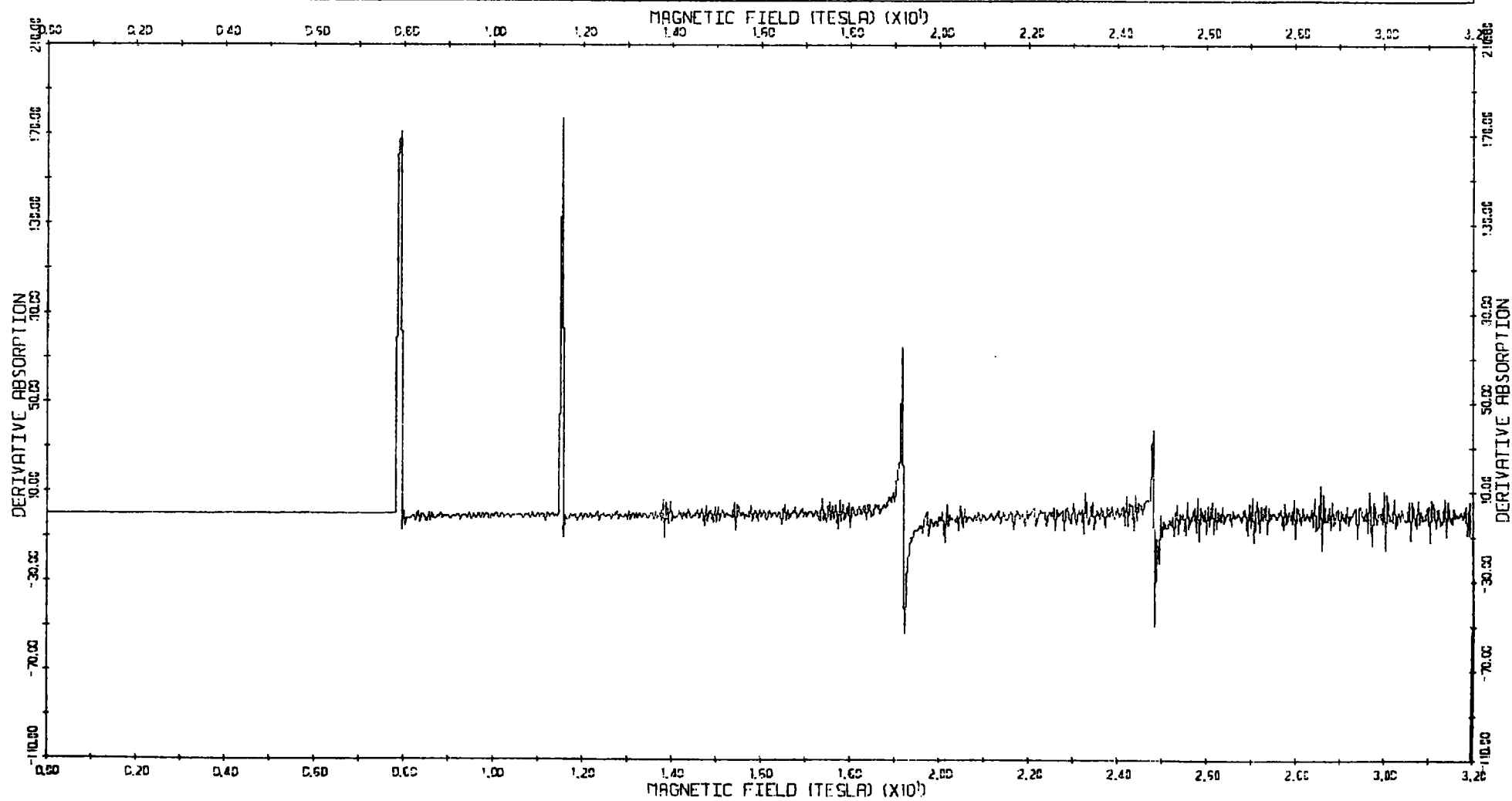


FIG. 7.16 E.S.R. POWDER LINE $\text{TiO}_2/\text{Fe}^{3+}$

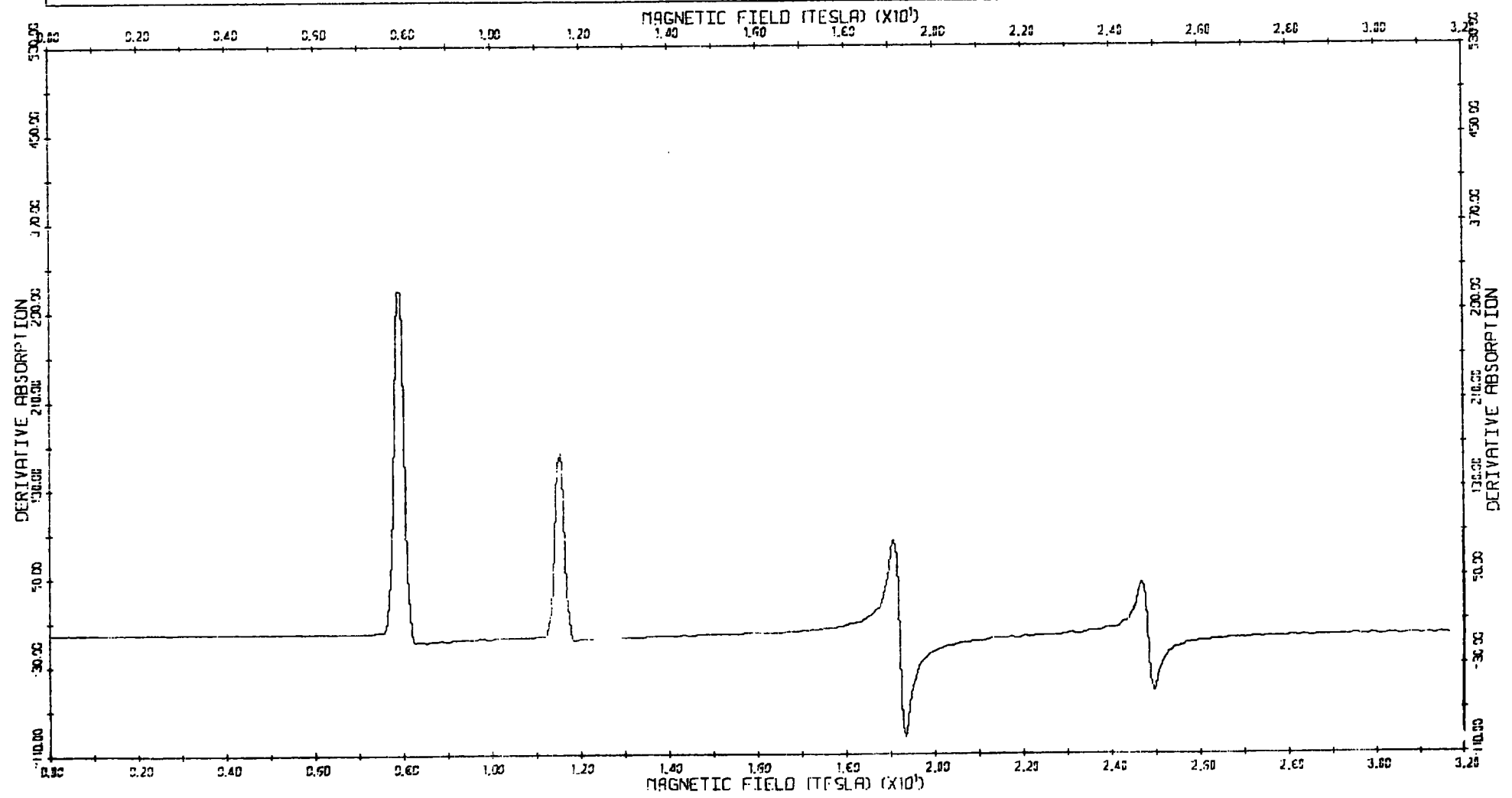
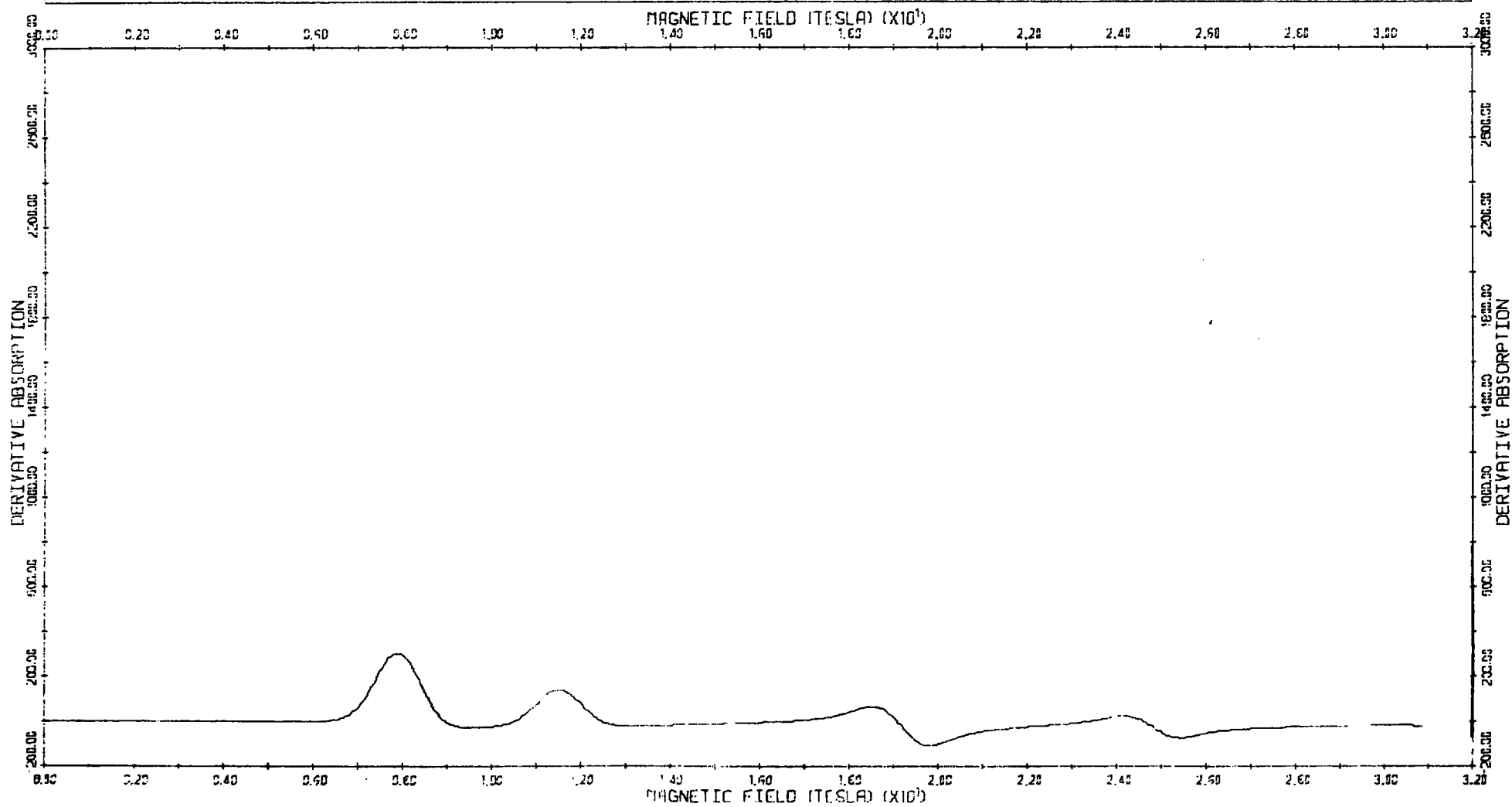


FIG. 7.17

E.S.R. POWDER LINE $\text{TiO}_2/\text{Fe}^{3+}$



Feature	Experimental Field mT	Calculated from numerical method (mT)	Calculated from Kneubuhl's method (mT)	Type	Principle values of Field for Fe/TiO ₂ (mT)
A	79.54	79.0	80.0	Step	79.1
B	115.59	115.2	117.5	Step	115.6
C	198.35	192.0	191.1	Peak	186.8
D	248.51	248.4	255.6	Peak	252.4
E	276.33	-	-	Peak	-
F	144	-	-	Peak	
G	314.4	-	-	Complex Peak	
		418.3	426.0	Small Step	412.0

TABLE 7.3 Comparison of observed and simulated Spectra.

effect of varying line intensities in more complex equations.

7.3.2 The Numerical Method

This gave reasonable agreement with experiments when the g^{-1} factor was included. No attempt was made to include a variation in the line intensity expected because the effective 'g' values of Fe/TiO_2 are very anisotropic because adequate simulations could be made without this complication. Several authors (7.4, 7.5, 7.6) have calculated the expected variation in intensity and this refinement could easily be included if desired.

7.3.3 General Conclusions

The work shows that the ESR powder spectra in the field range 0 to 0.5 Tesla at X band of Fe/TiO_2 can be treated as two independent transitions of effective spin $\frac{1}{2}$. At low temperatures (about 5K) the intensity of the transitions appears to vary as g^{-1} but at higher temperatures there appears to be a different behaviour. The features A and C are due to the $\pm \frac{1}{2}$ transition and B and D to the $\pm \frac{3}{2}$ transition. The expected feature at .420 mT was not seen but as it was so small in the simulations it could well be too small to be observed. The Spin Hamiltonian could be diagonalized for each orientation in the powder but this is not necessary in the region examined.

Work is continuing to understand the details of the variation in intensity of the lines with temperature and also to simulate the powder spectra of other ions using the same method.

In conclusion it may be said that the present work has shown that the simulation methods described do provide a satisfactory explanation of the main features of the ESR spectrum of powdered Fe/TiO_2 , although some problems remain in accounting for the detailed temperature variation of line intensity. As regards future work an immediate task would be to compute the powder spectra of other dopants in rutile ; here

the same method could be adopted simply using the parameters appropriate to the ion involved. The importance of thus building up a library of known powder spectra lies in the fact that the industrial pigments very rarely contain only one species of dopant. In the longer term a major question posed by the present work is that of the extent to which the intensity of a given feature in an ESR powder spectrum may be taken as representing the concentration of the species responsible for that feature. Time limitations have precluded examination of these topics.

REFERENCES

CHAPTER SEVEN -

- 7.1 F.K. Kneubuhl, 'Lineshapes of EPR Signals produced by Powders, Glasses and Viscous Liquids', J.Chem.Phys. 53 (1960) 1074.
- 7.2 R. Oasa and T. Vanngard, 'EPR Signal Intensity and Powder Shapes : A Re-examination', J.Magn.Reson. 19 (1975) 308.
- 7.3 F.K.Kneubuhl and B. Natterer, 'Paramagnetic Resonance Intensity of Anisotropic Substances and its Influence on Line Shapes'. Helv.Phys. Octa 34 (1961) 710.
- 7.4 J.R.Pelbrow, 'Anisotropic Transition Probability Factor in ESR' Mol. Phys. 16 (1964) 307.
- 7.5 F. Holey, 'The Spin Hamiltonian and Intensities of the ESR Spectra Originating from Large Zero Field Effects on States' Cam.J.Phys. 44 (1965) 503.
- 7.6 A. Isomoto, H.Watare, M.Kotani, 'Dependence of EPR Transition Probability on Magnetic Field', J.Phys.Soc. Japan, 29 (1970) 1571.

APPENDIX 1

RESULTS OF MASS SPECTROSCOPY OF SAMPLES

	National Lead Boule	Swiss (2) Boule		Tioxide International Pigments (2)		
		(centre)	(side)	A	C	E
% Al ₂ O ₃	1	0.007	0.03	0.61 ⁽³⁾	3.28 ⁽³⁾	1.56 ⁽³⁾
% SiO ₂	0.1	0.05	0.06	0.6	0.6	0.6
SO ₃	0.4	0.2	0.2			
% MgO	0.04	0.007	0.009	0.0006	0.002	0.0012
% Cl	0.01	0.003	0.009			
% Fe	0.01	0.05	1.5	0.0025	0.0035	0.0025
ppm K ₂ O	6	8	10	4	5	2
" CuO	20	20	200	10	15	8
" Sc ₂ O ₃	2	<2	<2			
" V ₂ O ₅	4	<2	<2	0.5	2	1
" Cr ₂ O ₃	≤6	≤10	≤8	1	2	2
" Mn O	2	<0.6	0.9	<0.2	0.3	<0.2
" Co O	<4	2	<2	<2	<2	<2
" NiO	≤10	≤9	≤20	≤3	-	-
" Cu	2	3	3	<1	3	<1
" ZnO	≤60	500	200	1	10	5
" Ga ₂ O ₃	<6	4	4			
" GeO ₂	≤30	≤20	≤40			
" As ₂ O ₃	1	2	2	35	4	1
" Se	6	6	6			
" Br	4	7	7			
" Rb ₂ O	4	≤30	≤20			
" SrO	≤0.8	6	80	<0.1	<0.1	<0.1

	National Lead Boule	Swiss (2) Boule		Tioxide International Pigments (2)		
		(centre)	(side)	A	C	E'
ppm Y_2O_3	1	0.6	40			
" ZrO_2	30	100	200	15	20	<2
" Nb_2O_5	10	20	20	4	2	4
" MoO_3	<6	≤9	≤9	<3	<3	<3
" Ag	8	0.5	0.5			
" Sn	2	<1	1	13	4	4
Ru		1	1			
Cd		<1	<1			
In		<0.3	<0.3			
ThO_2		<0.8	<0.8	12	2	<1
BaO		0.5	30	0.5	0.5	<0.5
La_2O_3		<0.4	0.5			
CeO_2		<0.5	1			
Pr_2O_3		<0.3	<0.3			
Nd_2O_3		<2	30			
Tu_2O_3		<1	<1	1	3	5
WO_3		<4	<4			
Hg		<2	<2			
Tl		0.7	<0.7			
Pb		<1	6			
Bi		10	500			
P_2O_5		800	300	8	25	8

- (1) See section 3.3(b) for explanation.
- (2) Pigments B,D and F are the same as A,C,E except that they have been heated at 600°C for 30 minutes.
- (3) These figures were obtained by chemical analysis and knowledge of the starting composition of the pigments. The results of the mass spectroscopy are

A 1% Al₂O₃

C 2% Al₂O₃

E 1.5% Al₂O₃

The difference reflects the inherent inaccuracies of mass spectroscopy especially at these relatively high concentrations.

